



140  
380  
THS

2  
2007

This is to certify that the  
dissertation entitled

THE STUDY OF SINGLE NANOPARTICLE AND MOLECULE  
PHYSICS

presented by

TIFFANY EVA BOHNSACK

has been accepted towards fulfillment  
of the requirements for the

Ph.D.

degree in

Chemical Engineering and  
Materials Science



Major Professor's Signature

12 June 2007

Date

LIBRARY  
Michigan State  
University

**PLACE IN RETURN BOX** to remove this checkout from your record.  
**TO AVOID FINES** return on or before date due.  
**MAY BE RECALLED** with earlier due date if requested.

<b>DATE DUE</b>	<b>DATE DUE</b>	<b>DATE DUE</b>

**THE STUDY OF SINGLE NANOPARTICLE AND MOLECULE PHYSICS**

**By**

**Tiffany Eva Bohnsack**

**A DISSERTATION**

**Submitted to  
Michigan State University  
in partial fulfillment of the requirements  
for the degree of**

**DOCTOR OF PHILOSOPHY**

**Department of Chemical Engineering and Materials Science**

**2007**

## ABSTRACT

### THE STUDY OF SINGLE NANOPARTICLE AND MOLECULE PHYSICS

By

Tiffany Eva Bohnsack

We intend to use cross-linked, polymeric nanoparticles as a device to store information when they are deformed (1) or in their native undeformed (0) state. To do this, information about the interaction between the nanoparticles and different surfaces must be determined. The substrates tested include a high energy mica surface and a low energy silanized silicon wafer. The nanoparticles collapse on the mica substrate, but remain robust and structured on the silanized wafer, yet an extreme amount of cross-linking is required for the nanoparticles to retain their original spherical shape regardless of the substrate surface energy. The nanoparticle behavior was also observed at elevated temperatures to reveal that the height of the extremely cross-linked nanoparticles slowly decreases. The temperature where a rapid size change occurs was well below the bulk glass transition temperature, suggesting unique phenomena at the nanoscale. The formation of ordered nanoparticle arrays is another essential aspect of molecular technology and can be produced by using single-wall carbon nanotubes as a template. Single wall carbon nanotubes serve as nucleation sites to focus nanoparticles toward them through strong van der Waals forces that are enhanced from geometrical effects. This interaction drives the nanoparticles to collect onto the nanotubes, which creates an alignment of nanoparticles onto carbon nanotubes. In final studies the nanoparticles were robustly attached to the surface through polymer film embedding. Embedding the

nanoparticles into a cross-linked thin polymer film locks the nanoparticles in place to prevent disruption of the nanoparticles during deformation.

## DEDICATION

This dissertation is dedicated to my parents, Larry and Diane Dukette, for their love, guidance, and help through all of my school years.

## ACKNOWLEDGEMENTS

There are many people that I would like to thank for their help and support during my graduate school studies. First, I would like to thank my advisor Professor Michael Mackay for his help and guidance during the research process. I am grateful to the members of the NIRT/CINCO team, specifically Karen Wooley and Brooke Van Horn for educating me in the details of the polymer synthesis involved in this research and Craig Hawker for providing the polystyrene nanoparticles used in my research. I would like to acknowledge Professor Phil Duxbury and Dr. Erin McGarrity for their discussions and help with the theory and physics entailed in this research. I would also like to thank my group members David Bohnsack, Melissa Holmes, Anish Tuteja, R.S. Krishnan, and Leslie Passeno for their help with laboratory experiments and research questions.

I would finally like to thank my family for all of their love and support throughout these years. I am profoundly grateful to my parents, Larry and Diane Dukette, and my brother and sister, Matthew and Kimberly Dukette, for helping me through all these years of college and supporting me and being there every step of the way.

## TABLE OF CONTENTS

LIST OF TABLES .....	vii
LIST OF FIGURES .....	viii
Chapter 1: Introduction .....	1
1.1 MOTIVATION FOR RESEARCH .....	1
1.2 RESEARCH BACKGROUND .....	3
Chapter 2: Conformation of Intramolecularly Cross-linked Polymer Nanoparticles on Solid Substrates .....	6
2.1 INTRODUCTION .....	6
2.2 EXPERIMENTAL .....	8
2.3 RESULTS AND DISCUSSION .....	12
2.4 CONCLUSION .....	21
Chapter 3: The behavior of individual polystyrene nanoparticles and macromolecules at elevated temperatures .....	22
3.1 INTRODUCTION .....	22
3.2 BACKGROUND .....	25
3.3 EXPERIMENTAL .....	27
3.3.1 <i>A Softening Effect Exhibited in Single Polystyrene Nanoparticles and Macromolecules</i> .....	27
3.3.2 <i>Thermal Conformation Changes of Polystyrene Macromolecules</i> .....	29
3.4 RESULTS AND DISCUSSION .....	31
3.4.1 <i>A Softening Effect Exhibited in Single Polystyrene Nanoparticles and Macromolecules</i> .....	31
3.4.1 <i>Thermal Conformation Changes of Polystyrene Macromolecules</i> .....	46
Chapter 4: Directional Self Assembly: Nanoparticles Drawn to Carbon Nanotubes .....	56
4.1 INTRODUCTION .....	56
4.2 EXPERIMENTAL .....	58
4.3 RESULTS AND DISCUSSION .....	61
4.4 CONCLUSION .....	70
Chapter 5: Embedding Nanoparticles into a Cross-linked Network .....	71
5.1 INTRODUCTION .....	71
5.2. EXPERIMENTAL .....	73
5.3. RESULTS AND DISCUSSION .....	76
5.4. CONCLUSION .....	83
Chapter 6: Conclusions .....	84
Appendix A: Atomic Force Microscopy .....	86
Appendix B: Height vs. Temperature Data for Polystyrene Macromolecules and Nanoparticles .....	91
References .....	97

## LIST OF TABLES

<b>Table 2.1</b> Sample, Molecular Mass, Polydispersity Index, Degree of Cross-Linking, Nature (i.e., linear precursor or cross-linked nanoparticle), and Diameter if the molecules collapse to the bulk density of polystyrene for the samples.....	9
<b>Table 3.1.</b> Sample, Molecular Mass, Polydispersity Index, Degree of Cross-linking, Nature (i.e. cross-linked or linear), and Diameter if the Macromolecules or Nanoparticles Collapse to the Bulk Density of Polystyrene (Eq.3.2) for the Samples. ....	27
<b>Table 4.1.</b> Sample Code, Number Average Molecular Weight (kD), Solvent, Diameter if the Macromolecules or Nanoparticles Collapse to the Bulk Density of Polystyrene and the AFM Height (Diameter) of Au and CdSe NPs.....	59
<b>Table 4.2.</b> Hamaker constants for typical substances used in our experiments.....	67
<b>Table 4.3.</b> Hamaker constants and energies for typical substances and geometries used in our experiments. ....	68
<b>Table 5.1.</b> Sample, Molecular Mass, Polydispersity Index (PDI), Degree of Cross-linking, Nature (i.e. cross-linked or linear), and Diameter if the Linear Precursors or Nanoparticles Collapse to the Bulk Density of Polystyrene (Eq.5.1) for the Samples. ....	74

## LIST OF FIGURES

- Figure 1.1.** Using nanoparticles as data storage for a nano-chemical reactor. Each nanoparticle can represent a bit of information. In its deformed state it represents a “1” and in its undeformed state it signifies a “0”. ..... 2
- Figure 2.1.** (a) Intramolecular cross-linking of polystyrene macromolecules is accomplished by opening a pendent cyclobutene (BCB) group and subsequent reaction cross-linking with a similarly activated group. The nanoparticles are produced by dripping a solution of linear-chain precursors into a hot solvent (benzyl ether) to activate the cross-linking process. (b) Example of the nanoparticle. The molecule is representative of a tightly cross-linked nanoparticle with every fifth monomer unit potentially cross-linked..... 9
- Figure 2.2.** (a) Atomic force microscopy height images of T-PS211k polystyrene nanoparticles on the mica substrate have an average height of  $2.9 \pm 0.1$  nm. The image lateral dimensions are  $3 \times 3 \mu\text{m}$ . (b) Atomic force microscopy height images of T-PS211k polystyrene nanoparticles on the Sigmacote™ substrate have an average height of  $9.3 \pm 0.2$  nm. The image lateral dimensions are  $3.5 \times 3.5 \mu\text{m}$ . (c) Should the nanoparticles adopt a spherical conformation on the substrate, then their height (H) should equal their diameter (D) which is 8.6 nm for the T-PS211k system (see Table 2.1). The nanoparticles may adopt a deformed shape on the substrate of equal volume to the sphere with a contact diameter d as described by the JKR theory..... 12
- Figure 2.3.** Height variation of lightly and tightly cross-linked nanoparticles (with different molecular weights) on substrates of high (a) and low (b) surface energy. The height values measured on the mica surface are much less than the predicted value, eq 2.1 (curve labeled  $H \sim M^{1/3}$ ), whereas the values measured on the Sigmacote™ surface approach the prediction of a spherical object for the tightly cross-linked nanoparticles. Height variation for three different moduli on the low-energy substrates is also shown (eq 2.6)..... 14
- Figure 2.4.** Height variation of two different cross-linked PS nanoparticles (20% and 60%), corresponding to the T-PS and E-PS systems, on high- and low-energy substrates. It can be seen that the E-PS system faintly changes shape on the high-energy (a) and low-energy (b) substrate. Height variation for three different moduli on the high and low free energy substrates is also shown (eq 2.6). A modulus of 3.2 GPa is the calculated modulus for the extremely cross-linked system using eq 2.8 as described in the text. Note the open triangle represents the height of the extremely cross-linked nanoparticle under the assumption that dimers are present within the system. .... 16
- Figure 3.1.** (a) A repeat scan of height versus temperature for the 393kD polystyrene macromolecules on Sigmacote™. Cycle 1 is the initial heights obtained at 25°C and 75°C and cycle 2 is the second observation of height versus temperature for the 393kD PS. In cycle 2 the macromolecules were heated from room temperature to 75°C in increments of 10°C. The AFM height of the macromolecules was measured at each temperature. A decrease in height is observed with a transition at approximately 40°C. Note that the large

error bars can be attributed to polydispersity and AFM error of 0.1 nm. (b) Distribution of height values from 25°C to 75°C for the cycle 2 values graphed in (a). .....	32
<b>Figure 3.2.</b> Surface tension vs temperature for polystyrene. <sup>25</sup> The surface tension of benzyl ether at 200°C is also shown and is much less than the surface tension of polystyrene in this temperature range (180°C – 240°C) to suggest that the polystyrene does not wet the substrate (Sigmacote™) at 200°C since the contact angle of benzyl ether on Sigmacote™ from 25°C to 200°C remains unchanged. ....	34
<b>Figure 3.4.</b> Should the nanoparticles adopt a spherical conformation on the substrate, then their height (H) should equal their diameter (D) which is 4.7 nm for the E-PS33kD system. The nanoparticles may adopt a deformed shape on the substrate of equal volume to the sphere with contact diameter d as described by the JKR theory.....	38
<b>Figure 3.5.</b> Modulus vs. temperature plot of 393kD polystyrene macromolecules on the silanized substrate and 33kD E-PS nanoparticles plotted from Eq. 3.8. The modulus for both systems was found for the second cycle values found on the silanized substrate. ...	41
<b>Figure 3.6.</b> For small values of $\alpha$ , the volume of the outer shell of monomers becomes a large fraction of a spherical particle's total volume fraction. ....	42
<b>Figure 3.7.</b> AFM heights of 33kD E-PS NPs measured at room temperature after 5 heat cycles to 75°C. Cycle 0 represents the initial height of the nanoparticles prior to heat. The nanoparticle height continuously decreases in height as the cycle number increases suggesting an increase in monomer adsorption to the substrate with each cycle .....	43
<b>Figure 3.8.</b> (a) Height of 393kD polystyrene macromolecules at room temperature after heating to the corresponding temperatures found on the graph. At 180°C the macromolecule's height increases significantly. (b) Height of 393kD PS macromolecules at room temperature after being heated to the corresponding temperatures on the graph. The height of the macromolecules fluctuates as the temperature is cycled between 75°C and 200°C. The raw data is shown as points to indicate the measurement errors caused by polydispersity. All heights were obtained by AFM. ....	48
<b>Figure 3.9.</b> (a) Average $R_g^2$ versus temperature for chains of length $N = 124$ . (b) Average macromolecule height from the surface as a function of temperature for $N = 124$ . From the inset, one can see the height begins to increase rapidly near $T_\theta$ . The scaled experimental data is shown with error bars for comparison. ....	51
<b>Figure 3.10.</b> $\langle R_0^2 \rangle / N$ versus temperature for different chain lengths ( $N= 64, 90, 124$ ). The crossing point for the length 90 and 124 chains gives a rough estimate of the $\theta$ temperature for the model, $T_\theta \approx 5.15$ . ....	53
<b>Figure 4.1.</b> AFM height images of (a) SWNTs spin coated onto a silicon wafer, (b) E-PS33kD NPs deposited from chloroform on mica (c) T-PS211kD NPs deposited from benzene on a silicon wafer (d) Au NPs deposited from toluene on mica. Note that for the AFM images in b,c, and d the SWNTs were deposited onto the selected substrate prior to nanoparticle deposition. ....	62
<b>Figure 4.2.</b> (a) and (b) TEM images of Au NPs aligned along SWNTs. (c) CdSe nanoparticles aligned along SWNTs and (d) T-211kD PS NPs agglomerated along SWNTs. ....	63

<b>Figure 4.3.</b> (a) Spherical nanoparticle (NP) diffusing in solvent near a nanotube (NT) on a substrate. (b-d) Coordinate systems for the geometries used in our systems: (b) sphere/sphere (c) sphere/plate and (d) sphere/cylinder. ....	65
<b>Figure 5.1.</b> (a) AFM height image of PS25kD film on Sigmacote™ after being heated to 250°C for 30 min. (b) Line analysis of the scratch made in the film. The film appears to be 4-5 nm thick. ....	77
<b>Figure 5.2.</b> (a) Diagram of nanoparticle embedded in thin polymer film. (b) Graph of the height of a T-PS211k nanoparticle on Sigmacote™ before embedment (black line) and the height of a nanoparticle after embedment (dashed line). The average difference in height between these particles is ~ 5-6 nm consistent with the film thickness determined in Fig. 5.1. ....	78
<b>Figure 5.3.</b> AFM height images of T-PS211k NPs embedded in a thin polymer film (PS25kD linear precursor). (a) Height image prior to cure (50 µg/mL). (b) Height image after heating to 250°C for 30 minutes (50 µg/mL). (c) Height image after the sample in bw was dipped in benzene for 1 minute (50µg/mL). (d) Height image after heating to 250°C for 30 minutes (100 µg/mL). (e) Height image after heating to 250°C for 30 minutes (200µg/mL). ....	79
<b>Figure A.1.</b> Atomic force microscopy diagram that illustrates the laser being emitted from the diode to the cantilever and reflected back to the detector. The feedback unit uses the input signal to produce the voltage that drives the piezoelectric ceramic. ....	86
<b>Figure A.2.</b> (a) Example of a good AFM phase image of 33kD E-PS NPs. (b) Example of a bad phase image of 33kD E-PS NPs. Some of the particles in the image appear triangular which indicates the tip is broken. The streaks that appear in the phase image indicate that either the surface is contaminated (e.g. finger print) or something is stuck to the tip such as a dust particle or nanoparticle. ....	87
<b>Figure A.3.</b> (a) AFM tip prior to tip approach. (b) AFM tip after tip approach. (c) AFM tip after scanning a mica substrate. (d) Damaged AFM tip. ....	88
<b>Figure A.4.</b> AFM heater design. Samples can be heated to a maximum temperature of 100°C without damaging the AFM. ....	89
<b>Figure A.5.</b> (a) AFM height image of nanoparticles aligned on single-walled nanotubes before tip approaches sample (b) AFM height image of nanoparticles aligned on single-walled nanotubes after tip approaches sample. In both (a) and (b) the black circle represents the targeted tip approach area and in (b) the dotted circle represents where the tip actually struck the sample. ....	90
<b>Figure B.1.</b> Height vs. temperature for 44kD polystyrene macromolecules heated from 25°C to 75°C. The sample was spray deposited from a solvent/non-solvent solution onto a silanized wafer. ....	92
<b>Figure B.2.</b> Height vs. temperature for 1.5MD polystyrene macromolecules heated from 25°C to 75°C. The sample was spray deposited from a solvent/non-solvent solution onto a silanized wafer. ....	92
<b>Figure B.3.</b> Height vs. temperature for 78kD T-PS nanoparticles heated from 25°C to 75°C. The sample was drop deposited onto a silanized wafer from benzene. ....	93

**Figure B.4.** Height vs. temperature for 211kD T-PS nanoparticles heated from 25°C to 75°C. The sample was drop deposited onto a silanized wafer from benzene. .... 93

**Figure B.5.** Height of 393kD PS macromolecules at room temperature after being heated to the corresponding temperatures on the graph. The height of the macromolecules fluctuates as the temperature is cycled between 75°C and 200°C. The graph shows the heights obtained after cycles 20 and 30. .... 94

**Figure B.6.** Height vs temperature graphs of the 211kD T-PS NP system. (a) NPs were deposited in pure benzene and (b) NPs were deposited in benzene/2-MEA. The nanoparticles do not undergo the same two phase behavior that is observed in the macromolecules..... 94

**Figure B.7.** FTIR spectrum of 393kD PS macromolecules directly after preparation. A 0.1 µg/mL solution of 70% benzene/30% 2-MEA was sprayed onto a silanized wafer. Only polystyrene peaks are present in the scan, there is no trace of residual solvent or non-solvent.....95

**Figure B.8.** XPS spectrum of 393kD PS macromolecules directly after preparation. A 0.1 µg/mL solution of 70% benzene/30% 2-MEA was sprayed onto a silanized wafer. The silanized wafer was used for the background. There is no trace of any residual solvent or non-solvent..... 96

## **Chapter 1: Introduction**

### **1.1 Motivation for Research**

Extensive research has been performed in the advancement of data storage systems at the nanoscale. The motivation for this research stems from the eventual application to the millipede.<sup>1-5</sup> The millipede is a recent innovation in nanomechanical data storage systems and consists of an array of cantilevers (64 x 64) and a micro-mechanical scanner that moves the storage medium (polymer film) relative to the array of cantilevers. With this system it is possible to read, write, and erase information within the polymer film. The millipede stores information by making an indentation into a polymer film with a heated atomic force microscopy (AFM) tip. Each indentation made into the polymer film creates a bit of information on the surface. In order to erase the bit the polymer film is reheated causing the polymer to soften and the stored elastic strain together with surface forces to relax. The array is supported by a 10 x 10 mm silicon wafer and can store greater than 1 terabit of information. To further advance this technology one could replace the polymer film with individual nanoparticles possibly allowing more information to be stored on a smaller area and decreasing fabrication problems, such as erasure of a single bit of information.

The concept of replacing the polymer film with an array of nanoparticles is investigated by studying the conformation of various nanoparticles and molecules. It is hypothesized that each individual nanoparticle represents a bit of information; i.e., “1” when deformed and a “0” in its initial state. An example of how this advancement of the millipede can be used is shown in Figure 1.1. The picture represents a nano-chemical reactor surrounded by lines of nanoparticles. These nanoparticles will then be used to

store information about the nano-chemical reactor by using “1”s and “0”s. A nanoparticle in its deformed state (“1”) is shown as a red particle and in its undeformed state (“0”) it is represented as a green particle.

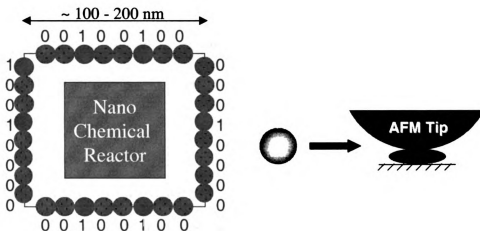


**Figure 1.1.** Using nanoparticles as data storage for a nano-chemical reactor. Each nanoparticle can represent a bit of information. In its deformed state it represents a “1” and in its undeformed state it signifies a “0”.

## 1.2 Research Background

In this work, we studied single polymer nanoparticle and molecule physics in order to accomplish use of this potential technology. First, we studied the substrate specific conformation of the nanoparticles. We recognize the initial conformation of nanoparticles on solid substrates, prior to deformation, is dictated by their intrinsic rigidity and interaction with a substrate which represents a critical aspect of this technology. The substrate free energy is changed by choosing a high energy surface, freshly cleaved mica, and a low energy surface, silanized silicon wafer.

Studying the nanoparticles' behavior at high temperature is also critical to this research. By observing an individual nanoparticle's or molecule's response to high temperatures we can understand thermal transitions that occur in a single molecule or nanoparticle. Quantifying a thermal transition of an individual molecule has been scarcely researched and rarely observed. Currently the only known way to determine a thermal transition of a single polymer molecule is by freeze drying an ultradilute solution with the molecule in its expanded state and then examining a differential scanning calorimetry (DSC) trace of the final product.<sup>6</sup> The first scan shows that an individual polystyrene molecule with molecular weight of  $1.8 \times 10^6$  Da has a glass transition temperature ( $T_g$ ) of 41°C and 60°C on the second and third scans. These temperatures are drastically lower than the  $T_g$  of bulk polystyrene which is 105°C. In the present study we provide information on the behavior of individual nanoparticles at high temperatures which is essential during the eventual deformation of the nanoparticles we will study on a substrate.

Atomic force microscopy (AFM) was used to study the conformation of nanoparticles on solid substrates at both ambient and elevated temperatures. AFM is a scanning-probe system that uses a sharp tip (probe) to scan over a sample while measuring local properties and creating a topographical image of the sample. Appendix A contains a detailed description of AFM and the methods used in all experiments described throughout this work.

Forming nanoparticle arrays is also an essential aspect in molecular technology. In past research, arrays of particles have been formed by using focused ion beam milling (FIB) to make patterns within a polymer film. Solutions of silicon dioxide particles were then deposited onto the patterned wafer and the particles arranged in forms similar to the patterned wafer.<sup>7</sup> In other studies, nanoparticles were aligned along nanoscale ridge-and-valley structured substrates.<sup>8,9</sup> In this research nanoparticle arrays are formed by aligning them against carbon nanotubes. Strong van der Waals interactions between a sphere (nanoparticle) and cylinder (nanotube) cause the nanoparticles to be drawn to the nanotubes. The nanoparticles collect onto the nanotubes creating a line of nanoparticles. By aligning the nanotubes on the surface one could potentially use this technique to create an array of nanoparticles.

In the final task, the nanoparticles were robustly attached to the surface to prevent tip forces from disordering the nanoparticle array during deformation. At the present time embedding the nanoparticles within a polymer film is the best way to achieve this.

Embedding nanoparticles into a cross-linked network of polymer film locks the particles into position on the substrate. The polymer film layer is thin enough so that the top of the nanoparticle is visible above the film. Researchers are currently exploring the

optical properties that are produced by embedding Ag nanoparticles into polymer films for metal/semiconducting polymer systems,<sup>10, 11</sup> but there is no current research being done on trapping a portion of the nanoparticles into a polymer film for molecular memory application.

## **Chapter 2: Conformation of Intramolecular Cross-linked Polymer Nanoparticles on Solid Substrates**

### **2.1 Introduction**

The first item addressed in this research is the substrate specific conformation of the nanoparticles. We recognize the initial conformation of nanoparticles on solid substrates, prior to deformation, is dictated by their intrinsic rigidity and interaction with a substrate which represents a critical aspect of this technology. The substrate free energy is changed by choosing a high energy surface, freshly cleaved mica, and a low energy surface, silanized silicon wafer.

The conformation of cross-linked, monomolecular, polystyrene nanoparticles on a solid substrate is studied here as a function of cross-linking degree and substrate surface energy.<sup>12</sup> It is found that an extreme degree of cross-linking is required for the ca. 5-10 nm diameter polystyrene nanoparticles to retain their original spherical shape, regardless of surface energy. The nanoparticles' rigidity is studied on a mica and silanized silicon wafer substrate. Both substrates are smooth at the Angstrom level thereby minimizing roughness effects on measurements.

It should be noted that the conformation of larger organic nanoparticles on solid substrates has been studied before by determining how they change size upon heating.<sup>13</sup> Also, in 1965, prior to present day atomic force microscopy, Richardson used scanning electron microscopy (SEM) to determine the molecular weight of individual molecules.<sup>14</sup> Polystyrene solution was sprayed onto a carbon-backed mica substrate and shadowed with deposits of gold and palladium. The shadow length for each molecule could then be determined through SEM images. To calculate the molecular weight of the individual molecules, it was assumed that the particles were spherical and that the diameter of the

particles was equal to their height. Due to limitations, there are two major difficulties in using this technique: defining the shadow limit cast by the spheres and the assumption of a spherical conformation on the substrate.

## 2.2 Experimental

Polystyrene nanoparticles were synthesized at IBM by Hawker, et al.<sup>15</sup> as illustrated in Figure 2.1. A linear random copolymer consisting of styrene monomer and benzocyclobutene (BCB) was first synthesized. The degree of cross-linking is dictated by the BCB content. We use three BCB levels: 2.5, 20, and 60 mol%, denoted as lightly (L), tightly (T), and extremely (E) cross-linked. A dilute solution of the linear precursor is then dripped into a hot solvent activating the intramolecular cross-linking reaction to create nanoparticles containing a single macromolecule whose size is dictated by the initial precursor molecular weight and the degree of cross-linking. The sample codes, molecular weights ( $M_n$ , number average molecular weight), polydispersity index (PDI, ratio of weight to number average molecular weight), and degree of cross-linking for the systems studied here are given in Table 2.1. The polystyrene nanoparticles' molecular weights were determined with a Wyatt "Dawn EOS" 18 angle static light scattering detector, and so are absolutely measured and not relative to calibration standards.

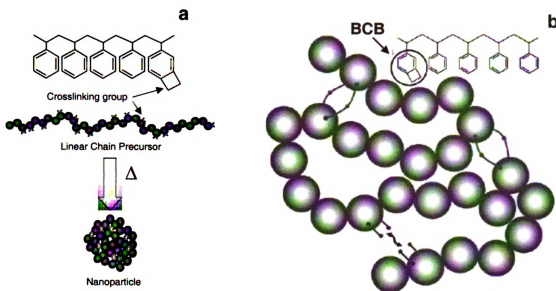


**Figure 2.1.** (a) Intramolecular cross-linking of polystyrene macromolecules is accomplished by opening a pendent cyclobutene (BCB) group and subsequent reaction cross-linking with a similarly activated group. The nanoparticles are produced by dripping a solution of linear-chain precursors into a hot solvent (benzyl ether) to activate the cross-linking process. (b) Example of the nanoparticle. The molecule is representative of a tightly cross-linked nanoparticle with every fifth monomer unit potentially cross-linked.

**Table 2.1** Sample, Molecular Mass, Polydispersity Index, Degree of Cross-Linking, Nature (i.e., linear precursor or cross-linked nanoparticle), and Diameter if the molecules collapse to the bulk density of polystyrene for the samples.

sample	Mn	PDI	mol % cross-linking agent	nature	diameter (nm)
PS33k	33.0	1.05	20	linear	4.7
PS58k	58.0	1.14	20	linear	5.6
PS193k	193	1.28	20	linear	8.4
L-PS25k	24.5	1.14	2.5	cross-linked	4.2
L-PS60k	60.1	1.16	2.5	cross-linked	5.7
L-PS158k	158	1.4	2.5	cross-linked	7.8
T-PS41k	41.0	1.04	20	cross-linked	5.0
T-PS78k	78.0	1.14	20	cross-linked	6.2
T-PS211k	211	1.32	20	cross-linked	8.6
E-PS33k	33.0	1.91	60	cross-linked	4.7

Surface profile measurements were performed with a Pacific Nanotechnology Nano-R atomic force microscope in close contact (oscillating) mode to generate height images that were not altered other than a simple leveling procedure. Silicon tips with a spring constant of 36 N/m, tip curvature of 10-20 nm, and a resonance frequency of 286-339 kHz were used for all experiments.

Sample preparation for AFM samples depended on the surface energy of the substrate. Freshly cleaved mica and silanized silicon wafer substrates were used for all experiments described below. The mica was cleaved and used immediately to avoid contamination from dust, atmospheric contaminants, and ionic crystals that are attracted to the surface due to mica's hydrophilic nature.<sup>16</sup> Because mica is a high free energy substrate, which most solvents will wet, solutions of sample were spin coated onto the mica at 5000 rpm for 40 seconds. The surface energy of the mica is dependent on its environment, with a value of ~4500 mN/m in high vacuum and ~300 mN/m in humid laboratory air.<sup>17</sup> The linear polymer precursors and nanoparticles were dissolved in benzene, and all solutions were filtered with a 0.2  $\mu\text{m}$  Teflon filter to reduce the amount of large dust particles and atmospheric contaminants prior to deposition.

Sigmacote<sup>TM</sup> was used to silanize the silicon wafers by spin coating the Sigmacote<sup>TM</sup> solution onto a silicon wafer at 5000 rpm for 40 seconds. Sigmacote<sup>TM</sup> (Sigma-Aldrich) is a solution consisting of 2.5% chlorosiloxane (( $\text{SiCl}_2\text{C}_4\text{H}_9$ )<sub>2</sub>O) and 97.5% heptane that functionalizes the surface with short alkane chains. The wafer was then rinsed with Millipore water to eliminate the excess, and then pure benzene was spin coated directly onto the wafer. The silanized wafer was then checked by AFM to ensure the coating provided a smooth surface containing no precipitates or dust particles. Due to

Sigmacote's™ low free energy surface (29 mN/m), the solutions could not be spin coated directly onto the surface and therefore a drop of solution (concentration, 0.01  $\mu\text{g/mL}$ ) was placed on the surface and exposed to air until the benzene had completely evaporated.

### 2.3 Results and Discussion

The nanoparticle heights were determined with AFM by taking the average of 50 particle heights; however, the lateral size could not be found due to convolution effects created by the tip.<sup>18, 19</sup> In Figure 2.2 an example of a three-dimensional AFM height image of the T-PS211k nanoparticles on the mica and Sigmacote™ substrates is shown. The image clearly demonstrates uniformity of nanoparticles on the surfaces and the narrow height distribution provides evidence that only individual polystyrene nanoparticles are present and no agglomeration of them occurs.

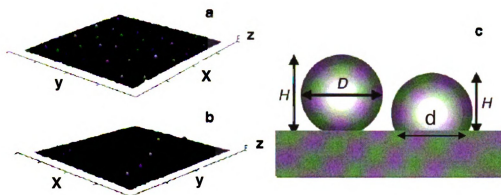


**Figure 2.2.** (a) Atomic force microscopy height images of T-PS211k polystyrene nanoparticles on the mica substrate have an average height of  $2.9 \pm 0.1$  nm. The image lateral dimensions are  $3 \times 3 \mu\text{m}$ . (b) Atomic force microscopy height images of T-PS211k polystyrene nanoparticles on the Sigmacote™ substrate have an average height of  $9.3 \pm 0.2$  nm. The image lateral dimensions are  $3.5 \times 3.5 \mu\text{m}$ . (c) Should the nanoparticles adopt a spherical conformation on the substrate, then their height ( $H$ ) should equal their diameter ( $D$ ) which is  $8.6$  nm for the T-PS211k system (see Table 2.1). The nanoparticles may adopt a deformed shape on the substrate of equal volume to the sphere with a contact diameter  $d$  as described by the JKR theory.

To ascertain the nanoparticle conformation on the substrate shown in Figure 2.2, we determine the diameter ( $D$ ) assuming the macromolecule collapses to a sphere with the bulk density of polystyrene ( $\rho \sim 1.04 \text{ g/cm}^3$ ) through

$$D = \left[ \frac{6M_n}{\pi N_A \rho} \right]^{1/3} \quad (2.1)$$

where  $N_A$  is Avogadro's number. The values are given in Table 2.1, and for sample T-PS211k, shown in Figure 2.2, the value of  $D$  (8.6nm) is much greater than its height on the high-energy substrate (the average height is  $2.9 \pm 0.1$  nm). Thus, on the mica surface the nanoparticles adopt a pancake-like conformation. This conformation is also observed in dendrimer structures where studies have shown that both charged and uncharged dendrimers adsorb to a mica surface forming a flat disk structure.<sup>20</sup>

To ensure that the height was not an AFM artifact caused by the cantilever drive amplitude (force), the amplitude was changed from 900 to 1500 mV when examining the T-PS211k nanoparticle sample. There was no change in the average nanoparticle height due to the equivalent pressure change, and therefore, it is suspected the high surface energy mica ( $\sim 300$  mN/m) is the most likely cause for the nanoparticles' collapse onto the surface. So, it is believed the set point or cantilever distance from sample did not play a role in these observations since the lowest possible setpoint was used for all AFM scans.

The effect of surface energy on the nanoparticle conformation is shown in Figure 2.3 and it is clear that the nanoparticles' height is affected. The solid line in each graph, labeled  $H \sim M^{1/3}$ , is a plot of eq 2.1 assuming the density is equal to that for bulk polystyrene. The height of the linear precursor macromolecules and lightly cross-linked nanoparticles are affected little by a change in the surface energy and fall below the value for a robust sphere. However, the tightly cross-linked nanoparticles show a drastic difference in the height profile with molecular mass and approach the scaling suggested

by eq 2.1 on the low-energy substrate, Sigmacote<sup>TM</sup>. So, there is a clear interaction between the substrate surface energy and nanoparticle stiffness implied through the degree of cross-linking.

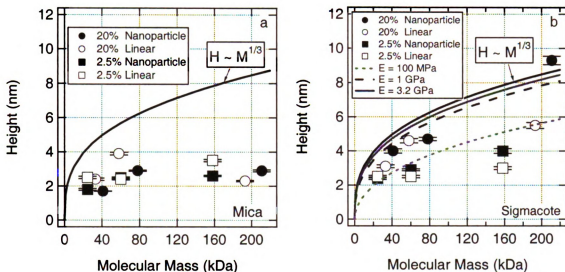


**Figure 2.3.** Height variation of lightly and tightly cross-linked nanoparticles (with different molecular weights) on substrates of high (a) and low (b) surface energy. The height values measured on the mica surface are much less than the predicted value, eq 2.1 (curve labeled  $H \sim M^{1/3}$ ), whereas the values measured on the Sigmacote<sup>TM</sup> surface approach the prediction of a spherical object for the tightly cross-linked nanoparticles. Height variation for three different moduli on the low-energy substrates is also shown (eq 2.6).

Since the T-PS series of nanoparticles collapses on the high energy mica substrate, a system was designed to ensure minimal collapse on any energy surface. This was done by recognizing the work of Chubynsky and Thorpe<sup>21</sup> who show a rigid network system is developed when the average coordination number  $\langle r \rangle$  is 2.4 in a cross-linked system. This value is determined by

$$\langle r \rangle = 2x_L + 3[1 - x_L] \quad (2.2)$$

where,  $x_L$  is the mole fraction of linear segments with coordination number 2 and  $1 - x_L$ , the mole fraction of cross-linked sites with coordination number 3. According to this theory, at least 40 mol % cross-linking, or two of every five monomer units, must be cross-linked to ensure rigidity. The extreme cross-linked system was designed to surpass this value with  $\langle r \rangle = 2.6$  where three of every five monomer units are cross-linked.

The extremely cross-linked nanoparticles were observed on both the high and low surface energy substrates and as shown in Figure 2.4 the nanoparticles slightly change shape on the high-energy substrate. For reference, the T-PS series is also shown in Figure 2.4 and it is clear that these nanoparticles are distorted on the high energy substrate. The open triangle is a representation of dimerization that could have occurred during synthesis of the extremely cross-linked nanoparticles. The experimental error observed in both Figures 2.3 and 2.4 could be due to the nanoparticle's polydispersity index (PDI) effect on the height. For the E-PS33k polystyrene nanoparticle series, it is found that the change in height based on PDI is 1.5 nm. The AFM height's experimental error is only 0.1 nm, which suggests the experimental error is mostly due to the nanoparticles' polydispersity. For a polydisperse system the molecular weight standard deviation ( $\delta M$ ) is given by  $M_n \times \sqrt{(\text{PDI}-1)}$  which can be used to calculate the error in the diameter ( $\delta D$ );  $\delta D/D = \delta M/3M$ , through propagation of error. Since the height data are influenced by small and discrete random effects, such as polydispersity index (PDI) and AFM error (~0.1 nm), the data can be normally distributed using the Central Limit Theorem (CLT). Using a sample size of 50, the CLT can be used to recognize that a distribution of an average approaches a normal distribution; thus, the normally distributed standard deviation ( $\sigma_x$ ) becomes

$$\sigma_x = \frac{\sigma_x}{\sqrt{N}} \quad (2.3)$$

where,  $\sigma_x$  is the non-normal standard deviation and  $N$  is the sample size. Thus, the error in the mean value ( $\sigma_x$ ) is the measured error ( $\sigma_x$ ) divided by the square root of the sample size ( $N$ ).

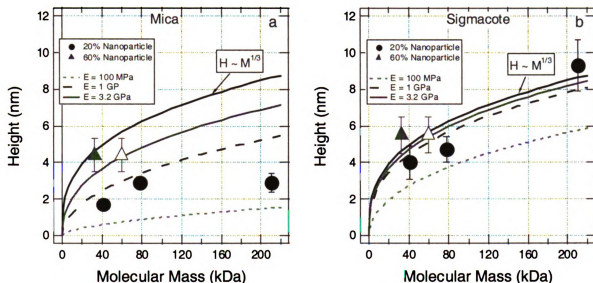


**Figure 2.4.** Height variation of two different cross-linked PS nanoparticles (20% and 60%), corresponding to the T-PS and E-PS systems, on high- and low-energy substrates. It can be seen that the E-PS system faintly changes shape on the high-energy (a) and low-energy (b) substrate. Height variation for three different moduli on the high and low free energy substrates is also shown (eq 2.6). A modulus of 3.2 GPa is the calculated modulus for the extremely cross-linked system using eq 2.8 as described in the text. Note the open triangle represents the height of the extremely cross-linked nanoparticle under the assumption that dimers are present within the system.

These results demonstrate that an extremely large degree of cross-linking is necessary to stabilize polymeric nanoparticles on the high-energy substrate suggesting a high modulus is required. Modeling of the linear polymer and nanoparticle conformation on the substrate can be achieved using the classic Johnson, Kendall, and Roberts (JKR) theory<sup>22</sup> and the assumption that the adsorbate geometry adopts a spherical cap shape

(Figure 2.2c). The JKR theory is an extension of the Hertz theory of elastic contact and is used to explain the adhesion between two elastic bodies under a compressive force. In the JKR theory it is assumed that elastic deformation must occur; however, studies performed by Kendall and Padgett have shown that the JKR theory applies to the coalescence behavior of latex particles even though large deformations are present and the material is not truly elastic.<sup>23</sup> Given this observation, we use the JKR theory for a sphere in contact with a flat surface, experiencing zero load, where the contact diameter (d) becomes

$$d^3 = 9\pi(1-\nu^2)\frac{W_A}{E}D^2 \quad (2.4)$$

with D being the predicted nanoparticle diameter (eq 2.1), E is Young's modulus,  $\nu$  is Poisson's ratio, and  $W_A$  is the work of adhesion given by

$$W_A = \gamma_A + \gamma_S - \gamma_{A/S} \approx 2(\gamma_A^d \gamma_S^d)^{1/2} \quad (2.5)$$

with  $\gamma$  being the surface energy of the adsorbate-vapor (A), substrate-vapor (S), and adsorbate-substrate (A/S) interfaces. The approximation is due to Fowke's relation<sup>24</sup> that is applicable to lower energy substrates that interact through dispersive forces (the superscript d represents the dispersive part of the surface energy or tension). In our case, polystyrene<sup>25</sup> interacts via dispersive forces and has  $\gamma_A^d = 40$  mN/m while the silanized substrate has  $\gamma_S^d \approx 28.6 \pm 0.6$  mN/m at room temperature.

As stated above, the adsorbate geometry is assumed to be either a spherical cap or a disk with equal (constant) density between the sphere (see eq 2.1) and the adsorbed shape (see Figure 2.2c). For the spherical cap geometry one finds

$$d_s^3 = \frac{8}{3\sqrt{3}} \frac{(D^3 - H^3)^{3/2}}{H^{3/2}} \quad (2.6)$$

where H is the adsorbate's height on the substrate. Combining the JKR theory and the spherical cap, one can determine the interrelation between the nanoparticle height and surface and molecular properties

$$H^3 + kH - D^3 = 0 \quad (2.7)$$

where

$$k = \left[ \frac{27\pi\sqrt{3}}{8} (1-\nu^2) \frac{W_A}{E} D^2 \right]^{2/3}$$

By solving for H, with varying D, we were able to generate height-molecular weight relations for different modulus values as shown in Figure 2.4. Note that this model only corresponds to the nanoparticles and linear precursors that have not collapsed.

The E-PS series can be further investigated since these nanoparticles exhibit minimal collapse on the low- and high-energy surfaces. Due to this phenomenon we can assume  $D \approx H$  and therefore  $[D - H] \rightarrow 0$ . Using Eq. 2.7 and the assumed limit, H can be expressed as

$$H = D \left[ 1 - \frac{C}{C_r^{2/3}} \right] \quad (2.8)$$

where

$$C_r = \frac{ED}{W_A(1-\nu^2)} \text{ and } C = \left( \frac{9\pi}{8} \right)^{2/3}$$

The term  $C_r$  in eq 2.8 refers to the crumble number, which was developed by Kendall and Padgett, to serve as a guideline for the coalescence behavior of dispersed elastic particles. The crumble number can be used to determine whether a latex film will become porous and opaque ( $C_r > 10$ ) or tough, transparent, and nonporous ( $C_r < 1$ ).<sup>23</sup> Using this expression for the two substrates (labeled 1 and 2 for mica and Sigmacote™), one finds

$$\frac{H_2 - H_1}{D} = -C \left[ \frac{1}{C_{r2}^{2/3}} - \frac{1}{C_{r1}^{2/3}} \right] \quad (2.9)$$

Assuming  $\nu = 0.5$  then the modulus is the only unknown parameter and we find  $E \approx 3.2$  GPa. It is shown in Fig. 2.4 that a model curve with a modulus of 3.2 GPa corresponds well with the height value for the E-PS series on either substrate, especially for the case of possible dimerization. Further, the modulus for the E-PS series proves to be approximately equal to that for bulk polystyrene ( $\approx 3$  GPa), traditionally determined with tensile testing or with an AFM.<sup>26</sup> This may be expected due to the extreme degree of cross-linking, yet, the system is a single molecule and hence may be subject to finite size effects.

We can also estimate the modulus for T-PS nanoparticles by noting that they exhibit minimal collapse on the low energy substrate. Assuming  $C_r > 10$  for this system (eq. 2.8) we estimate  $E > 100$ -150 MPa, where in fact we find  $E = 1$  GPa agrees fairly well with the height data (Fig. 2.3). Thus, increasing the degree of cross-linking 3-fold produces a change in the modulus by about a half-order of magnitude.

The L-PS and T-PS, as well as the linear precursor polymers collapse on the substrates, particularly on the high energy mica. To understand why their height becomes so small ( $\approx 3$  nm) and essentially independent of molecular weight we consider the work of Rubinstein and co-workers who studied single chain adsorption on surfaces,<sup>27</sup> with an

emphasis on the adsorption of polyelectrolytes on charged surfaces.<sup>28, 29</sup> If the surface is weakly adsorbing then the number of monomer units in contact with the surface will increase in order to gain adsorption energy; therefore, the chain height on the substrate will be smaller than its unperturbed size and lose conformational entropy. This phenomenon is observed on the mica substrate for the L-PS and T-PS nanoparticle systems where the number of monomer units within the nanoparticle that are in contact with the surface must increase causing the nanoparticles to spread out onto the surface into a pancake-like conformation. The size of the adsorption blob ( $\xi_{ads}$ ), which is equivalent to the chain height on the substrate, can be estimated by knowing the number of monomers in each adsorption blob that are in contact with the surface and each individual adsorption blob's energy gain estimated through

$$\delta k_B T \left( \frac{\xi_{ads}}{b} \right)^2 \approx k_B T \quad (2.10)$$

where  $\delta k_B T$  is the thermal energy gain of each individual monomer in contact with the surface. Here  $b$  represents the Kuhn monomer length, which is 1.8 nm for polystyrene. Assuming  $\xi_{ads} \approx H$ , one can find the adsorption energy per monomer for a linear polymer or collapsed nanoparticle ( $H \approx 3$  nm, see Fig. 2.3) to be  $\approx 0.5k_B T$ . Since dispersion forces are  $\approx k_B T$  in strength this estimate of the adsorption blob-substrate interaction energy is expected as is the adsorbate conformation.

## **2.4 Conclusion**

After investigating the interaction between nanoparticles on a low and high energy substrate, it was determined that the conformation of nanoparticles changes significantly. It was discovered that the L-PS and T-PS series collapse forming a pancake-like conformation on a high energy substrate with an adsorption energy adequately described by a theory developed for linear polymer systems. Conversely, on the low energy substrate, the T-PS and E-PS series form robust spherical objects with a height that corresponds to their molecular weight. Yet, the modulus is estimated to be a half-order of magnitude larger for the E-PS system. Further, only the E-PS molecule does not significantly collapse on either substrate demonstrating an extremely rigid network is required for the nanoparticle to retain its shape regardless of substrate surface energy. Since the motivation for this work requires a deformable nanoparticle, it is clear that extreme cross-linking cannot be used and so the interplay of substrate surface energy and nanoparticle modulus must be carefully considered.

## **Chapter 3: The behavior of individual polystyrene nanoparticles and macromolecules at elevated temperatures**

### **3.1 Introduction**

The behavior of polystyrene nanoparticles and macromolecules was observed at elevated temperatures to reveal that the height of the particles slowly decreases. The temperature where a rapid size change occurs was well below the bulk glass transition temperature suggesting unique phenomena at the nanoscale. A softening effect that occurs in individual nanoparticles and macromolecules can be determined via AFM by observing the height of the nanoparticles at different temperatures using an AFM hot stage. In this work we found a softening point that occurs at  $\sim 40^{\circ}\text{C}$  for all polystyrene nanoparticles and macromolecules. This softening point is attributed to the scale of a single nanoparticle and macromolecule from that of the bulk. The JKR theory is used to study the change in modulus of the particles as the surface tension of polystyrene changes with temperature.

Thermal transitions of individual macromolecules are scarcely researched experimentally because of the difficulty imposed by the length scales involved. Currently, the only known way to determine the thermal transition of a single polymer macromolecule is by freeze drying an ultra-dilute solution with the macromolecule in its expanded state and then examining a differential scanning calorimetry (DSC) trace of the final product. Xue, et al.,<sup>30</sup> used this technique to suggest that an individual polystyrene macromolecule with molecular weight of  $1.8 \times 10^6$  D has a glass transition temperature ( $T_g$ ) somewhere between  $40^{\circ}\text{C}$  and  $60^{\circ}\text{C}$ . These temperatures are drastically lower than the  $T_g$  of bulk polystyrene which is  $105^{\circ}\text{C}$ .

A lower glass transition temperature has also been observed in thin film studies. The Tg of thin polymer films has been extensively studied using x-ray reflectivity, ellipsometry, reflection absorption FTIR, and dielectric and x-ray photoelectron spectroscopy.<sup>13, 31-37</sup> In these studies it is found that as the polymer film thickness decreases the glass transition temperature becomes less than that of the bulk polymer. In recent work, Torkelson et al. used intrinsic fluorescence to study the Tg of thin polymer films in their equilibrated state and showed that nano-confinement effects cause Tg of the polymer to decrease from the bulk Tg in both equilibrium and non-equilibrium states.<sup>31</sup> In this work low temperature experiments in the range 25°C - 75°C will be discussed to reveal a softening effect that occurs within macromolecules and nanoparticles well below the bulk Tg of the polymer.

High temperature experiments (~200°C) were also conducted. In the high temperature experiments it was observed that a single macromolecule exhibits a two phase behavior between the temperatures of 75°C and 200°C. At 200°C a single macromolecule can be thermally stimulated to explore the half-space above the substrate and is experimentally shown to be in an extended conformational state. The macromolecule can fluctuate between this extended state at 200°C and collapsed state at 75°C and so it may be possible to develop a data storage device by thermally stimulating single macromolecules between compact and extended states.

Property measurement of single macromolecules at the nanometer scale has only become possible in recent years.<sup>6, 38</sup> These macromolecules exhibit two conformational states: a collapsed state at low temperatures and an expanded state at high temperatures. In this work we use a combination of experiment and Monte Carlo molecular simulation

to examine and explain this unusual and never before demonstrated behavior. The height was independent of the molecular weight (size) of the nanoparticles. Similar behavior is expected for single linear (uncross-linked) chains on the surface. Flory-type calculations and scaling theory predict that single chains adsorbed onto substrates from solution will have essentially two-dimensional conformations whose height is also found to be independent of molecular weight.<sup>27</sup>

### 3.2 Background

In a previous study<sup>12</sup> it was discovered that nanoparticles with a low degree of cross-linking spin coated onto a substrate will adopt a pancake shape due to van der Waals force exerted by the surface (see Chapter 2). Single polystyrene macromolecules will also adopt this adsorbed shape when spin coated in pure benzene. To explain this adsorbed height, we considered Rubinstein and co-workers' work on the study of single chain adsorption to understand why a polystyrene nanoparticle or macromolecule height becomes so small (~ 3nm) and essentially independent of molecular weight.<sup>27,28,29</sup> The adsorption theory can be used to show that the chain will exchange part of its conformational entropy for the energy it gains by adsorbing to the surface thereby collapsing onto the substrate. The conformation of larger organic particles on solid substrates has been studied before by determining how they change size upon heating.<sup>13</sup> These larger core-shell nanoparticles reversibly change shape upon thermal treatment from a disk to a sphere conformation. At temperatures below the melting temperature of the crystalline core the particles adopt a disk-like structure and above this melting temperature the particles adopt a spherical structure.

Richardson used scanning electron microscopy (SEM) to determine the molecular weight of single macromolecules.<sup>14</sup> Polystyrene solution was sprayed onto a carbon-backed mica substrate and shadowed with deposits of gold and palladium. The shadow length for each macromolecule could then be determined through SEM and this length was then assumed to be related to the height of the macromolecule on the substrate. To calculate the molecular weight of the individual macromolecules, it was also assumed that the particles were spherical and that the diameter of the particles was equal to their

height. Due to limitations, there are two major difficulties in using this technique: defining the shadow limit cast by the spheres and the assumption of a spherical conformation on the substrate.

In order to prevent the macromolecules from collapsing on the substrate, Richardson used a precipitant/solvent solution. Adsorption of the uncross-linked macromolecules was minimized here using Richardson's method<sup>14</sup> by spraying a solution consisting of a solvent and non-solvent (precipitant) where the non-solvent has a higher surface tension than the substrate as well as a low vapor pressure. Using this technique the macromolecules still collapse substantially on the substrate, but they do not collapse to their adsorbed height when spin coating from a good solvent alone. This method increases the macromolecule height by ~2 nm and we use it in the present study to understand how a macromolecule, which is not strongly adsorbed onto a substrate, changes conformation.

### 3.3 Experimental

#### 3.3.1 A Softening Effect Exhibited in Single Polystyrene Nanoparticles and Macromolecules

The polystyrene macromolecules were standards purchased from Scientific Polymer Products, Inc. The weight average molecular weights used in the experiments were 44 kD, 393 kD and 1.5 MD and the polydispersity indices (PDIs) of the polystyrene standards are 1.07, 1.16, and 1.03, respectively. We prepared ultra-dilute solutions of the polystyrene ( $0.001\mu\text{g/mL}$ - $20\mu\text{g/mL}$ ) in pure benzene or a mixture of benzene and 2-methoxyethylacetate (2-MEA).

Polystyrene nanoparticles were synthesized according to the procedure of Harth, et al.<sup>15</sup> and kindly provided by Prof. Craig Hawker. A detailed description of the nanoparticles characteristics, including molecular weights and polydispersity index can be found in previous work<sup>12</sup> (see Chapter 2) and are given in Table 3.1.

**Table 3.1.** Sample, Molecular Mass, Polydispersity Index, Degree of Cross-linking, Nature (i.e. cross-linked or linear), and Diameter if the Macromolecules or Nanoparticles Collapse to the Bulk Density of Polystyrene (Eq.3.2) for the Samples.

sample	$M_n$ (kDa)	PDI	mol % cross-linking agent	nature	diameter (nm)
PS41k	41.0	1.07	0	linear	5.0
PS339k	339.0	1.16	0	linear	10.1
PS1530k	1530.0	1.03	0	linear	16.7
T-PS78k	78.0	1.14	20	cross-linked	6.2
T-PS211k	211.0	1.32	20	cross-linked	8.6
E-PS33k	33.0	1.91	60	cross-linked	4.7

Surface profile measurements were performed with a Pacific Nanotechnology Nano-R atomic force microscope in close contact (oscillating) mode to generate height images that were not altered other than a simple leveling procedure. Silicon tips with a spring constant of 25-75 N/m, tip curvature of <10 nm, and a resonance frequency of

200-400 kHz were used for all experiments. The nanoparticle heights were determined by taking the average of 50 nanoparticle heights; however, the lateral size could not be found due to convolution effects created by the AFM tip.<sup>18,19</sup> A hot stage was designed for the Nano-R AFM so that individual macromolecules and nanoparticles could be observed at elevated temperatures. The hot stage consisted of a solid metal cylindrical sample puck with an alumina insulator, heater element, and thermocouple connected to a PID controller to monitor the temperature (see Appendix A, Figure A.4). AFM scans at temperatures above room temperature require that the hot stage be turned off during scanning due to electrical interference effects; therefore, the high temperature experiments have a temperature range of approximately  $\pm 5^{\circ}\text{C}$  as the heater cools slightly during AFM scans. In all elevated temperature experiments the sample and AFM components were kept at the desired temperature for  $\sim 3$  hours to ensure that all components, specifically tip and sample, had reached the desired temperature, which aided in the prevention of thermal drift.

The polystyrene macromolecules were prepared in a solution of 30% 2-MEA and 70% benzene and sprayed onto a silanized substrate using a Meinhard nebulizer (model TR-30-A1). In this case the benzene is expected to quickly evaporate leaving a single polystyrene chain in a drop of 2-MEA which is a non-solvent for polystyrene. The 2-MEA drop will deposit on the substrate and slowly evaporate, leaving a macromolecule that does not completely collapse.

The silanized substrate (Sigmacote<sup>TM</sup>) was chosen for these experiments because it has a lower surface energy ( $\approx 29$  mN/m) than the surface tension energy of 2-MEA ( $\approx 34$  mN/m) and therefore the 2-MEA will not wet the substrate. If the 2-MEA had wetted

the substrate it would have caused the macromolecule to collapse to an adsorbed state of 3nm as we confirmed by other non-solvents such as n-butanol, which has a surface tension energy of ~25 mN/m.

Sigmacote™ was used to silanize the silicon wafers by spin coating the Sigmacote™ solution onto a silicon wafer at 5000 rpm for 40 seconds. Sigmacote™ (Sigma-Aldrich) is a solution consisting of 2.5% chlorosiloxane ((SiCl<sub>2</sub>C<sub>4</sub>H<sub>9</sub>)<sub>2</sub>O) and 97.5% heptane that functionalizes the surface with short alkane chains. The wafer was then rinsed with Millipore water to eliminate the excess. The silanized wafer was checked by AFM to ensure the coating provided a smooth surface with an RMS roughness below 0.5 nm.

Solutions of polystyrene nanoparticles were prepared in benzene at concentrations of 1 – 10 µg/ml and either deposited by allowing a drop of solution to evaporate onto a silanized substrate or spin coated onto a freshly cleaved mica substrate. Mica is a high surface energy substrate (≈ 300 mN/m). The nanoparticles were not sprayed onto the substrates because a better dispersion of particles can be obtained with spin-coating and drop deposition. Also, since Richardson's method does not affect the nanoparticles spraying them onto the substrate was not necessary.

### **3.3.2 Thermal Conformation Changes of Polystyrene Macromolecules**

The polystyrene (PS) macromolecules were standards purchased from Scientific Polymer Products, Inc. The weight average molecular weight used in the experiments was 393kD with a polydispersity index (PDI) of 1.16. We prepared ultra-dilute solutions of the polystyrene (0.001µg/mL - 20µg/mL) in pure benzene or a mixture of benzene and

2-methoxyethylacetate (2-MEA). All solutions were filtered with a 0.2 $\mu$ m Teflon filter to reduce the amount of atmospheric contaminants prior to deposition.

Surface profile measurements were performed with a Pacific Nanotechnology Nano-R atomic force microscope in close contact (see section 3.3.1 for details).

### 3.4 Results and Discussion

#### 3.4.1 A Softening Effect Exhibited in Single Polystyrene Nanoparticles and Macromolecules

In this section we will look at two distinct phenomena that occur for the polystyrene macromolecules and nanoparticles. Both systems appear to become less rigid at higher temperatures by exhibiting a softening effect at  $\sim 40^\circ\text{C}$ . These systems also undergo a partial adsorption to the substrate with each heat cycle.

**Low Temperature Experiments for Polystyrene Macromolecules.** The heights of individual polystyrene macromolecules were measured at temperatures ranging from  $25^\circ\text{C}$  to  $75^\circ\text{C}$ . Scans were repeated for three heating cycles. In Figure 3.1a the measured heights of 393kD PS macromolecules at room temperature and at higher temperatures by increments of  $10^\circ\text{C}$  up to  $75^\circ\text{C}$  is shown. After being heated to  $75^\circ\text{C}$ , the sample was slowly cooled down on the AFM hot stage to room temperature and then re-measured to determine if they recover to their initial deposited height.

A height decrease and a transitional temperature are obvious in all the samples. After heating to  $75^\circ\text{C}$  and measuring the height at room temperature it can be seen that they do not completely recover their original height. This same phenomenon was observed in the 44kD and 1.5MD polystyrene macromolecules (see Appendix B, Figures B.1 and B.2). Note that the large error bars in Figure 3.1 can be attributed to the polydispersity of the macromolecules to yield a height standard deviation ( $\delta h$ ) of  $\pm 1\text{nm}$ . For a polydisperse system the molecular weight standard deviation ( $\delta M$ ) is given by

$$\delta M = M_n \times \sqrt{(PDI - 1)} \quad (3.1)$$

which can be used to calculate the error in the diameter of an assumed spherical morphology ( $\delta D$ );  $\delta D/D = \delta M/3M$ , through propagation of error. This effect comes from measuring different sets of particles on each repeat scan since the AFM probe can not be precisely positioned at the same place for each temperature. The per-particle error is limited by the AFM instrument and is about 0.1nm as we confirmed by analyzing a single macromolecule repeatedly. The results in Figure 3.1b show the distribution of the data where the mean (Figure 3.1a) and the highest and lowest values all suggest a height decrease with increasing temperature.

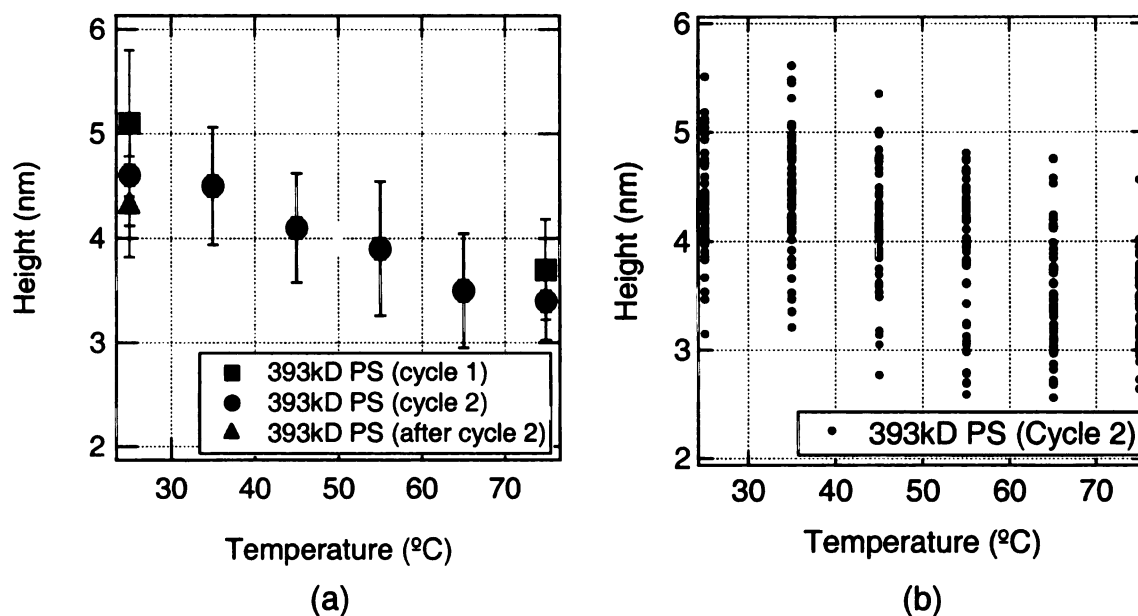


**Figure 3.1.** (a) A repeat scan of height versus temperature for the 393kD polystyrene macromolecules on Sigmacote™. Cycle 1 is the initial heights obtained at 25°C and 75°C and cycle 2 is the second observation of height versus temperature for the 393kD PS. In cycle 2 the macromolecules were heated from room temperature to 75°C in increments of 10°C. The AFM height of the macromolecules was measured at each temperature. A decrease in height is observed with a transition at approximately 40°C. Note that the large error bars can be attributed to polydispersity and AFM error of 0.1 nm. (b) Distribution of height values from 25°C to 75°C for the cycle 2 values graphed in (a).

The unusual phenomenon exhibited in Figure 3.1a was carefully investigated. Initial concerns were centered on the possibility of residual solvent (esp. 2-MEA) remaining in the sample and influencing the height behavior. Fourier transform infrared spectroscopy (FTIR) and X-ray photoelectron spectroscopy (XPS) were performed to prove that 2-MEA was not present in the sample after initial preparation (see Appendix B, Figures B.7 and B.8). The possible role of surface energy dependence on temperature was also investigated. Advancing and receding contact angle measurements were performed on a Sigmacote™ surface at 25°C and 200°C using benzyl ether (boiling point ~298°C) and it was found that the contact angle remained unchanged. The surface tension of benzyl ether<sup>39</sup> from 25°C to 200°C changes from 36 mN/m – 23 mN/m and since the surface tension of polystyrene at these temperatures (40mN/m – 27mN/m) is larger than the surface tension of the benzyl ether the polystyrene will not wet the substrate (see Fig. 3.2). So, the height decrease appears to be the result of a transition within the macromolecule itself.

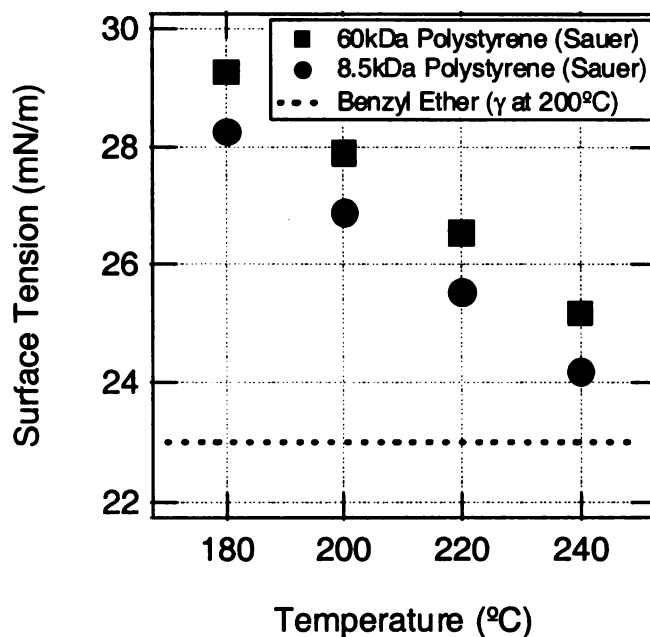


**Figure 3.2.** Surface tension vs temperature for polystyrene.<sup>25</sup> The surface tension of benzyl ether at 200°C is also shown and is much less than the surface tension of polystyrene in this temperature range (180°C – 240°C) to suggest that the polystyrene does not wet the substrate (Sigmacote™) at 200°C since the contact angle of benzyl ether on Sigmacote™ from 25°C to 200°C remains unchanged.

**Low Temperature Experiments for Polystyrene Nanoparticles.** The nanoparticles that were investigated for these experiments included the 78kD T-PS, 211kD T-PS, and 33kD E-PS nanoparticles (Table 3.1). The L-PS series was not studied because this system collapses on both the high and low energy substrates regardless of the solvent treatment during spin coating. The solvent/non-solvent technique (Richardson's method) was performed on the cross-linked systems, specifically the L-PS series, and it was discovered that the height of the particles changed minimally from the heights discussed below. The nanoparticle systems contain loops of monomer units that are connected by cross-links. These loops are thought to be more easily adsorbed to the surface than the freely-jointed chain in a macromolecule. This suggests that Richardson's

technique only affects the uncross-linked polystyrene macromolecules described above and not the cross-linked systems.

In Fig. 3.3a a graph of the thermal behavior for the 33kD E-PS system is displayed for both the high surface energy (mica) and low surface energy substrates (Sigmacote™). See Appendix B, Figures B.3 and B.4 for temperature graphs of the 78kD T-PS NP and 211kD T-PS NP systems. The 33kD E-PS system was studied in more detail due to its high degree of cross-linking, which prevents the nanoparticle from collapsing on both low and high free energy substrates when deposited from solution. In both cases there is a softening temperature at approximately 40°C proving that surface energy of the substrate does not play a role in the height decrease, which suggests that this decrease in height as temperature increases is solely due to a temperature effect within the polystyrene system. Note that in thin film studies it was found that the interfacial energy between the polymer and substrate altered the glass transition temperature of the polymer thin film.<sup>37</sup> Contrary to our results, they found polymer films on lower surface free energies exhibit a T<sub>g</sub> below the bulk T<sub>g</sub>, whereas films on higher surface free energies exhibit a T<sub>g</sub> above the bulk T<sub>g</sub>. Note that after being heated to 75°C and cooling down to room temperature the nanoparticle does not completely regain its original shape. The other nanoparticles in the T-PS series also exhibit a similar behavior; therefore, all systems studied for both nanoparticles and macromolecules have a softening temperature around 40°C regardless of molecular weight or degree of cross-linking.

One element to take into consideration despite the results of our previous XPS and FTIR studies is the possibility that residual benzene is present within the macromolecules and evaporates as temperature is increased, thus causing the nanoparticle

to shrink. In order to study this behavior a second cycle was performed on the nanoparticles to ensure that the nanoparticle will undergo the same behavior and with the assumption that any residual benzene is no longer present and the system is in equilibrium. In cycle 2 the height of the nanoparticle decreases as temperature increases and again has a thermal transition at approximately 40°C. This behavior is graphed in Figure 3.3b. After the second cycle the nanoparticle is slowly cooled down to room temperature and re-imaged. The height appears to be only slightly less than the initial height of the nanoparticle at room temperature for the second cycle. An additional experiment was performed to determine if the nanoparticle will continuously decrease from its initial height. The sample was heated for five cycles to 75°C for one hour and then measured via AFM once the sample had completely cooled down. The sample gradually decreased in height with each cycle suggesting that the nanoparticle is slowly adsorbing on the substrate and gaining molecular contact despite its high degree of cross-linking.

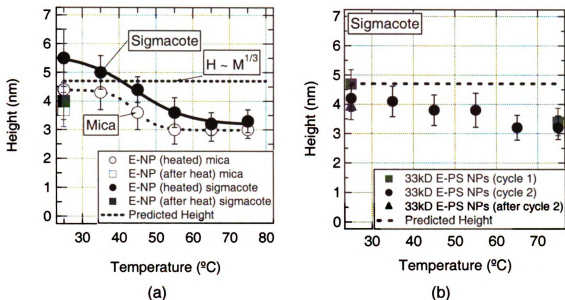


**Figure 3.3.** (a) Height vs temperature graph for 33kD E-PS system on mica and Sigmacote™. A softening temperature of approximately 40°C is observed for the nanoparticles on both substrates, suggesting that surface energy does not play a role in this transitional temperature. (b) Height vs temperature graph for 33kD E-PS system on Sigmacote™ for 2 cycles. For both (a) and (b) the macromolecules were heated from room temperature to 75°C in increments of 10°C. The height of the macromolecules was measured at each temperature. A decrease in height is observed with a transition at approximately 40°C.

Polystyrene nanoparticles and macromolecules exhibit the same softening effect at temperatures slightly above 40°C. The graphs in Figures 3.1 and 3.3 reveal that molecular weight, cross-linking degree, and substrate surface energy do not affect the softening effect at ~40°C. Since these factors can be eliminated as a cause for this we are lead to further examine the effect of the surface tension of polystyrene.

As temperature is increased the surface tension of the polystyrene is decreased, which will cause the polystyrene to maximize its contact with the silanized wafer with a concomitant decrease in height. In Dee and Sauer's work<sup>25</sup> they showed that the surface tension of polystyrene decreases as temperature increases, but the surface tension of

polystyrene does not fall below the surface energy of the silanized wafer until approximately 200°C; thus, suggesting that below 200°C the polystyrene will not wet the substrate. Yet, we can consider the small decrease in the surface tension of polystyrene between 25°C and 75°C and see how it can cause a height decrease using the JKR model.

The JKR theory<sup>22</sup> can be utilized to understand how surface tension affect the nanoparticles and macromolecules adsorption. The JKR theory is a model that describes the adhesion between two bodies under a compressive force and accounts for the short-ranged surface forces acting inside the contact area. The theory is based on the Hertzian theory yet takes into consideration the adhesion in the contact zone. We can examine this softening effect by observing the modulus change of the adsorbate through the use of the JKR theory and the assumption that the adsorbate geometry adopts a spherical cap shape (see Fig. 3.4). Note that for the JKR model the contact geometry is allowed to deform, which accounts for the nanoparticle and macromolecule collapse or deformation as temperature increases.

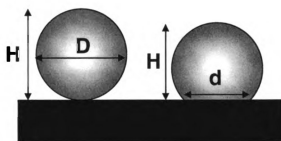


**Figure 3.4.** Should the nanoparticles adopt a spherical conformation on the substrate, then their height ( $H$ ) should equal their diameter ( $D$ ) which is 4.7 nm for the E-PS33kD system. The nanoparticles may adopt a deformed shape on the substrate of equal volume to the sphere with contact diameter  $d$  as described by the JKR theory.

To ascertain the nanoparticle conformation on the substrate shown in Figure 3.4, we determine the diameter (D) assuming the macromolecule collapses to a sphere with the bulk density of polystyrene ( $\rho \sim 1.04 \text{ g/cm}^3$ ) through

$$D = \left[ \frac{6M_n}{\pi N_A \rho} \right]^{1/3} \quad (3.2)$$

where  $N_A$  is Avogadro's number.

We use the JKR theory for a sphere in contact with a flat surface, experiencing zero load, where the contact diameter (d) becomes

$$d^3 = 9\pi(1-\nu^2) \frac{W_A}{E} D^2 \quad (3.3)$$

with D being the predicted nanoparticle and macromolecule diameter (eq 3.2), E is Young's modulus,  $\nu$  is Poisson's ratio, and  $W_A$  is the work of adhesion given by

$$W_A = \gamma_A + \gamma_S - \gamma_{A/S} \approx 2(\gamma_A^d \gamma_S^d)^{1/2} \quad (3.4)$$

with  $\gamma$  being the surface energy of the adsorbate-vapor (A), substrate-vapor (S), and adsorbate-substrate (A/S) interfaces. The approximation is due to Fowke's relation<sup>24</sup> that is applicable to lower energy substrates that interact through dispersive forces (the superscript d represents the dispersive part of the surface energy or tension). In our case, polystyrene<sup>25</sup> interacts via dispersive forces and has  $\gamma_A^d = 40 \text{ mN/m}$  while the silanized substrate has  $\gamma_S^d \approx 28.6 \pm 0.6 \text{ mN/m}$  at room temperature. As mentioned earlier the surface energy of the silanized substrate was found to be constant for temperatures up to 200°C.

For higher temperatures the surface tension of polystyrene can be determined from the equation<sup>25</sup>

$$\gamma_{PS} = 41.5 - 0.068T \quad (3.5)$$

where surface tension ( $\gamma$ ) is measured in mN/m and T is measured in °C.

As stated above and in previous work<sup>12</sup>, the adsorbate geometry is assumed to be a spherical cap with equal (constant) density between the sphere (see eq. 3.2) and the adsorbed shape (see Fig. 3.1). The volume of the spherical cap geometry is expressed as

$$V_{cap} = \frac{\pi}{6} H \left( 3 \left( \frac{d_{cap}}{2} \right)^2 + H^2 \right) \quad (3.6)$$

Analyzing the spherical cap geometry with equal (constant) density between the sphere (see eq. 2) and the adsorbed shape (see Figure 3.1) we find

$$d^3 = \frac{8}{3\sqrt{3}} \frac{(D^3 - H^3)^{\frac{3}{2}}}{H^{\frac{3}{2}}} \quad (3.7)$$

where H is the adsorbate's height on the substrate. Combining the JKR theory and the spherical cap geometry (eq. 3.3 and 3.7), we can determine the interrelation between the nanoparticle height and surface energy

$$H^3 + \left[ \frac{27\pi\sqrt{3}}{8} (1-\nu^2) \frac{W_A}{E} D^2 \right]^{\frac{2}{3}} H - D^3 = 0 \quad (3.8)$$

Taking the surface tension change of the polystyrene with temperature (eq. 3.5) we examine how modulus of the macromolecules and nanoparticles changes with temperature shown in Fig. 3.5. In Fig. 3.5 we see a decrease in modulus as temperature increases suggesting a softening effect is occurring in both macromolecules and

nanoparticles. The modulus values shown in Fig. 3.5 were measured for the second cycle values of each system (Fig. 3.1a and 3.3b) to ensure the systems had reached equilibrium. Note the modulus of the macromolecules is less than that of the nanoparticles. This difference in modulus is due to the rigidity of the nanoparticles, which is caused by the large degree of cross-linking (60%).<sup>12, 21</sup> The modulus of the E-PS NP system for cycle 2 on Sigmacote™ at 25°C is  $\approx 1.5$  GPa, which is approximately half the modulus of bulk polystyrene ( $E \approx 3$  GPa). This is due to partial adsorption to the substrate after the initial cycle.

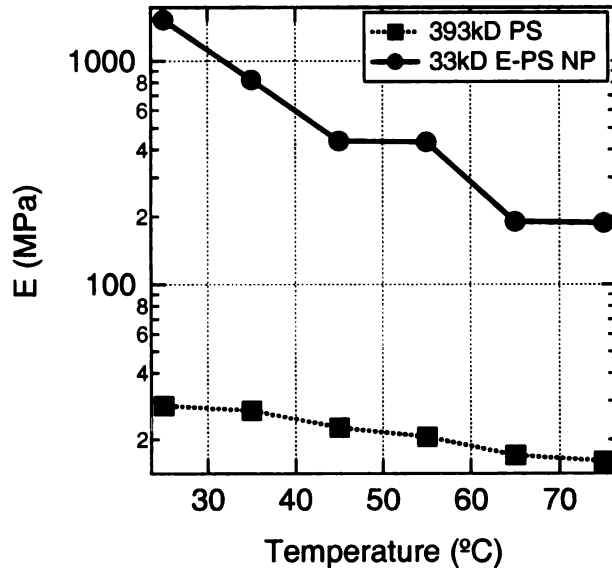


**Figure 3.5.** Modulus vs. temperature plot of 393kD polystyrene macromolecules on the silanized substrate and 33kD E-PS nanoparticles plotted from Eq. 3.8. The modulus for both systems was found for the second cycle values found on the silanized substrate.

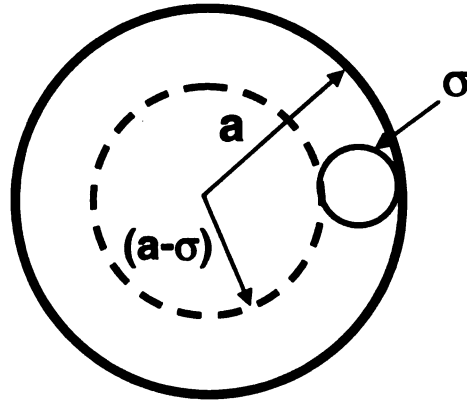


**Figure 3.6.** For small values of  $\alpha$ , the volume of the outer shell of monomers becomes a large fraction of a spherical particle's total volume fraction.

To understand in more detail why the macromolecules and nanoparticles soften and collapse from their kinetically trapped metastable conformations below the glass transition,  $T = 40^\circ\text{C} \ll T_g$ , we need to examine the scale of the problem. Consider a simple model where the surface elements of a single polymer chain collapsed into a spherical globule (see Fig. 3.6). We simplify this further by ignoring the chain bonding elements and examine only the van der Waals forces between Kuhn monomer units. The volume of a layer of monomer units on the surface is given by

$$S_s = \frac{4\pi a^3}{3} \left( 1 - \left( 1 - \frac{\sigma}{a} \right)^3 \right) \quad (3.9)$$

where  $\sigma$  is the Kuhn monomer diameter and  $a$  is the radius of the globule. Dividing this by the volume of the sphere ( $4\pi a^3/3$ ) we find the fraction of monomers on the surface. For a nanoparticle of radius  $a = 5\text{nm}$  and thermal blob size  $s = 1\text{nm}$  we have,

$$\frac{S_s}{V_s} = 1 - 0.8^3 \approx 0.5 \quad (3.10)$$

or half of the monomer units are on the surface. These surface monomer units experience less van der Waals force than the ones in the center, because they have less surrounding neighbors than internal monomers, and so one may expect the energy required to remove one of these external monomer units is quite a bit less, say one-half the energy of one from the bulk of the globule. We hypothesize this has the effect of reducing the temperature at which the particle can be deformed plastically by an external force below its bulk  $T_g$ .

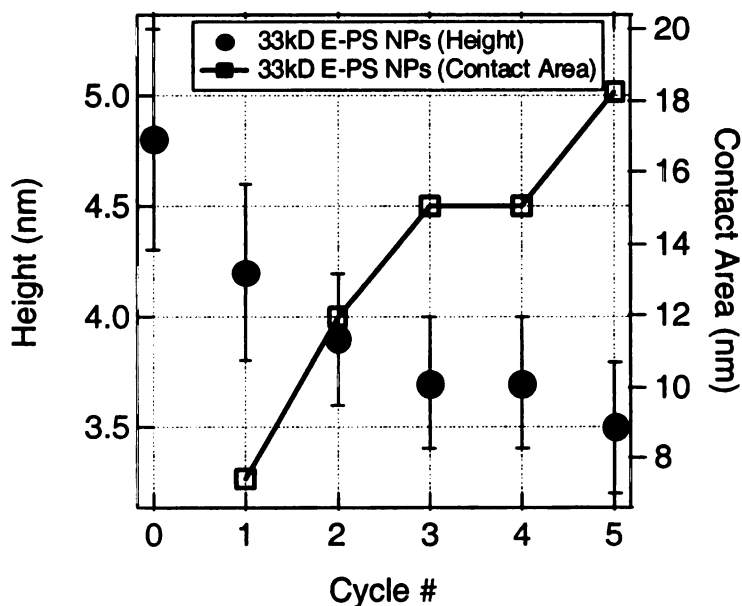


**Figure 3.7.** AFM heights of 33kD E-PS NPs measured at room temperature after 5 heat cycles to 75°C. Cycle 0 represents the initial height of the nanoparticles prior to heat. The nanoparticle height continuously decreases in height as the cycle number increases suggesting an increase in monomer adsorption to the substrate with each cycle.

We also need to consider that the macromolecules and nanoparticles gradually adsorb to the substrate after being heated to 75°C. As mentioned earlier, the E-PS NPs continuously collapse after 5 cycles to a height of approximately 3.5 nm, suggesting that the nanoparticles will eventually collapse to their adsorbed height of 3 nm.<sup>27</sup> Fig. 3.7 contains a graph of the AFM height values of the 33kD E-PS NPs measured after being heated to 75°C for 5 cycles. The contact area after each temperature cycle is also graphed in Fig. 3.7 and is determined by assuming constant density and a spherical cap geometry (eq. 3.7). After each temperature cycle more monomer units are in contact with the substrate which prevents the nanoparticle from returning to its initial conformation as the chain cools down to room temperature.

To understand this collapse transition, we study the equilibrium state of the nanoparticles in solvent and in air. The nanoparticles are initially deposited onto the substrate by weak adsorption from solvent. While in the solvent, they adopt ideal configurations, from which we may estimate their height off the substrate with the help of a scaling theory.<sup>27</sup> When the solvent evaporates, the particles become trapped in non-equilibrium conformation by their glassy character and connectivity constraints. This results in chain configurations that extend off the substrate higher than their equilibrium adsorption blob height in air. To collapse completely requires the particle to undergo massive changes in their conformations, which occurs during repeat heat cycles.

We begin by calculating the height for an adsorbed nanoparticle in air using the de Gennes method.<sup>27, 40</sup> In this case, the nanoparticle should be completely collapsed, since air is a non-solvent for PS. The average volume fraction of adsorption blobs with  $g_{\text{ads}}$  monomers is given by

$$\phi \approx \frac{b^3 g_{ads}}{\epsilon_{ads}^3} \approx 1, \quad (3.11)$$

where  $\epsilon_{ads}$  is the adsorption blob size, and  $b$  is the Kuhn monomer length. In the collapsed case all the monomers in the adsorption blob are in the attractive well of the surface so  $g_{ads} = (\epsilon_{ads}/b)^3$ . The number of Kuhn monomers in contact with the surface can be determined from

$$n_a \approx \frac{\phi}{b^3} \epsilon_{ads}^2 b \approx \frac{\epsilon_{ads}^2}{b^2}. \quad (3.12)$$

The macromolecule exchanges conformational entropy for adsorption energy by being in contact with the surface. The energy gain is written as

$$\delta k_B T \frac{\epsilon_{ads}^2}{b^2} \approx k_B T, \quad (3.13)$$

where  $\delta$  is the adsorption strength (for weak adsorption  $\delta < 1$ ). Solving for  $\delta$  we find

$$\delta \approx \frac{b^2}{\epsilon_{ads}^2}. \quad (3.14)$$

From our previous work<sup>12</sup> the adsorption blob size of a polystyrene macromolecule or nanoparticle in air is,  $\epsilon_{ads} \sim 3\text{nm}$ . Using  $b \sim 1.8\text{nm}$  as the Kuhn length for polystyrene, we find  $\delta \sim 0.36$ . Using  $\delta$  to compute the height,  $\epsilon$ , of the nanoparticles in solvent for ideal and real chain statistics,<sup>27</sup> we find

$$\epsilon \approx \frac{b}{\delta} \approx 5\text{nm} \text{ (ideal) and } \epsilon \approx \frac{b}{\delta^{3/2}} \approx 8\text{nm} \text{ (real)}, \quad (3.15)$$

which can be used for lower and upper estimates of height immediately after solvent evaporation. This is in very good agreement with the AFM height on the substrate measured directly after deposition of the 33kD E-PS nanoparticles onto the substrate.

After each heating cycle, the nanoparticles gradually adsorb until they reach their equilibrium state in air. This is graphed in Figure 3.7, where we see that after each heat cycle the nanoparticles are gradually decreasing in height or adsorbing to the substrate.

### **3.4.1 Thermal Conformation Changes of Polystyrene Macromolecules**

A two phase behavior in single polystyrene macromolecules examined on a solid substrate at elevated temperatures was also studied. A fluctuation between an extended state at 200°C and a collapsed state at 75°C is observed using atomic force microscopy measurements and Monte Carlo simulations.

In our first experiment, the substrates were heated in an oven for 30 minutes to six different temperatures ranging from 100°C to 200°C and then cooled for measurement at room temperature. As the macromolecules cool they collapse partially, but a signature of their high temperature extended state remains. This phenomenon was further investigated to determine if the macromolecules could be thermally annealed into completely adsorbed states. The macromolecules' heights were measured after repeated heating cycles between 75°C and 200°C.

The results from these experiments are shown in Fig. 3.8a and b. Each point on these graphs is an average of 50 measured particles. The error bars were computed using the standard deviation of the mean since this accounts for the polydispersity in our sample. In the first experiment (Fig. 3.8a), the macromolecules seem to have the same height upon cooling until the heating temperature reaches 180°C, at which point, they freeze into a taller configuration. We believe this extended height is an indication the particles are undergoing a molecular reordering.

The heights cycled between the two temperatures are shown in Fig. 3.8b, where it is seen that in the initial cycles the fluctuations between the two states are large, until cycle 4, after which they appear to stabilize into a two state system. Subsequent measurements beyond cycle 7 showed similar oscillations (the macromolecules were taken through 30 cycles total- see Appendix B, Fig. B.5).

The observed height change in these single macromolecules is remarkable. In order to explain our findings it is important to illuminate the differences between our experiments and the null experiment (macromolecules deposited with pure solvent). The main difference is the starting state, which, in the case of our experiments is non-equilibrium. When the chains are deposited, they are in a partially pinned state where trains of monomers<sup>41</sup> are strongly adsorbed to the surface. This combined with the chain constraints results in a high energetic barrier to relaxation and subsequent adsorption.

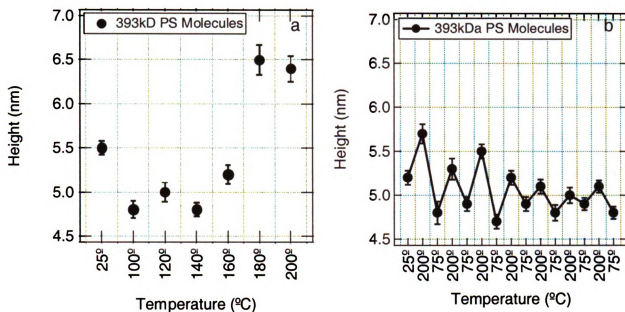


**Figure 3.8** (a) Height of 393kD polystyrene macromolecules at room temperature after heating to the corresponding temperatures found on the graph. At 180°C the macromolecule’s height increases significantly. (b) Height of 393kD PS macromolecules at room temperature after being heated to the corresponding temperatures on the graph. The height of the macromolecules fluctuates as the temperature is cycled between 75°C and 200°C. The raw data is shown as points to indicate the measurement errors caused by polydispersity. All heights were obtained by AFM.

To gain some insight into the possible chain conformations on the substrate, and into the cause of the “pop up” observed in the experiments, we performed Monte Carlo (MC) simulations<sup>42-44</sup> of an on-lattice, interacting, self-avoiding walk (ISAW)<sup>45</sup> near an attractive substrate<sup>46, 47</sup>. Previous simulation studies generated possible phase diagrams for single chains near a surface<sup>48, 49</sup>, but did not examine the heights of the macromolecules.<sup>i</sup>

<sup>i</sup> Dr. Erin McGarity performed the Monte Carlo simulations described here.

Similar simulations have been done for isolated single chains in bulk to study the globule to coil transition, which occurs as the temperature is raised from below to above the  $\theta$  temperature,  $T_a^{47}$ . The phase behavior of single chains becomes more complicated in the presence of a surface since the chains will adsorb on the surface at temperatures lower than the adsorption transition temperature,  $T_a$ . The phase behavior is fairly well understood for  $T_a > T_\theta$ , but not for  $T_a < T_\theta$  since polymer solutions phase separate at low temperature<sup>50</sup>. However, this is not an issue here since we have single chains isolated on the substrate in air. We expect that since air is a poor solvent for PS, the chains will undergo their globule to coil transition at lower temperatures than those at which the chains would desorb from the substrate, i.e. we expect that  $T_a > T_\theta$  in our case.

We chose to use a 12-connected lattice for our simulation because of its algorithmic simplicity and speed and because the packing on such a lattice resembles a hard sphere solid at low temperatures. The ISAWs were sampled using a variant of the pruned- enriched Rosenbluth method (PERM)<sup>51, 52</sup> and ensemble averaged over a wide range of normalized temperatures ( $k_B T/e = 0.25 - 20$ ). The energy of the chains is given by

$$U_{chain} = -\frac{1}{2} \sum_{k=1}^N (\epsilon c_k + \epsilon_s s_k) + \frac{1}{2} \sum_{k=2}^N \epsilon_g g_k \quad (3.16)$$

where  $\epsilon$  is the monomer-monomer attractive energy and  $\epsilon_s$  is the monomer-surface interaction energy.  $N$  is the chain length and  $c_k, s_k$  are the counts of contacts of the monomer at site  $k$  with the other monomers and the surface, respectively. Finally,  $\epsilon_g$  is a bending energy term and  $g_k$  is a Boolean variable which takes on the value 0 for trans- and 1 for gauche- angles between bonds  $(k + 1, k)$  and  $(k, k-1)$ . This model is a hybrid of those used by Doye et al.<sup>47</sup> and Bachmann et al.<sup>48</sup>.

The model parameters were chosen so that the ratio  $\epsilon/\epsilon_s$  was similar to the experimental system. The surface tension of PS is  $\approx 40$  mN/m, while the surface energy of the silanized substrate is  $\approx 29$  mN/m. We set  $\epsilon/kT = 1$  and thus took  $\epsilon_s/kT = 0.25$ . PS is fairly flexible so we modeled it as a floppy chain with  $\epsilon_g/kT = 0.05$ .

Once the chains were grown, statistics were computed at each temperature using the usual procedure<sup>53-55</sup>,

$$\langle X \rangle = \sum_{k=1}^z W_k X_k \quad (3.17)$$

where  $z$  is the number of chains including its Boltzmann factor and degeneracy, and  $X_k$  is the variable of interest for chain  $i$ . It is important to note that only chains which touched the substrate with at least one monomer unit were included in these averages. We thus did not attempt to find the desorption transition for our model. The averages were calculated using  $z \sim 10^8$  samples at each temperature below 10 and  $z \sim 10^7$  for the rest ( $k_B T/\epsilon > 10$ ). The additional sampling at low temperature is to account for the poor efficiency of the chain growth algorithm in the dense regime.

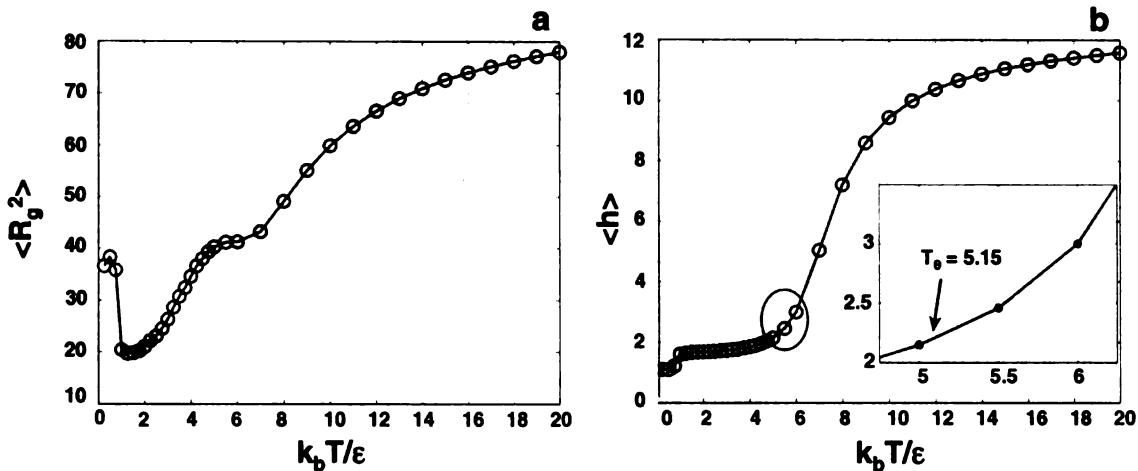


**Figure 3.9.** (a) Average  $R_g^2$  versus temperature for chains of length  $N = 124$ . (b) Average macromolecule height from the surface as a function of temperature for  $N = 124$ . From the inset, one can see the height begins to increase rapidly near  $T_g$ . The scaled experimental data is shown with error bars for comparison.

Our simulation shows a range of behaviors, as can be seen from the average radius of gyration ( $R_g$ ) and the average molecular height off the substrate ( $h$ ) of the macromolecules as functions of temperature, shown in Fig. 3.9 a and b. At low temperatures the chains are in rod-like configurations ( $R_g^2 \sim N^2$ ) adsorbed to the surface. As the temperature is increased, the macromolecules collapse into 2D adsorbed globules, with  $R_g^2 \sim N^{2/3}$  and small values of  $h$ . Further increases in temperature cause the chain to spread out on the surface, with  $R_g^2$  increasing but  $h$  staying nearly constant at the adsorption blob size. Near a temperature of  $T \approx 5$ , the chains undergo their globule to coil transition and adopt ideal random walk configurations,  $R_g^2 \sim N$ , while still adsorbed on the surface. Finally, they begin to desorb from the surface for  $T \geq 6$  and adopt ideal ( $R_g^2 \sim N$ ) and swollen configurations ( $R_g^2 \sim N^{6/5}$ ), with  $R_g$  and  $h$  increasing with both  $T$  and chain length.

The globule to coil transition is found by following the technique outlined by Binder et al.,<sup>56</sup> in which the  $\theta$  temperature is estimated from the crossover scaling of chains of different lengths. In Fig. 3.10, we plot the normalized squared end-to-end distance  $\langle R_0^2 \rangle / N$  versus temperature. The inset shows that the longest chains cross at  $T \approx 5.15$ , which we take as  $T_\theta$  for our model.

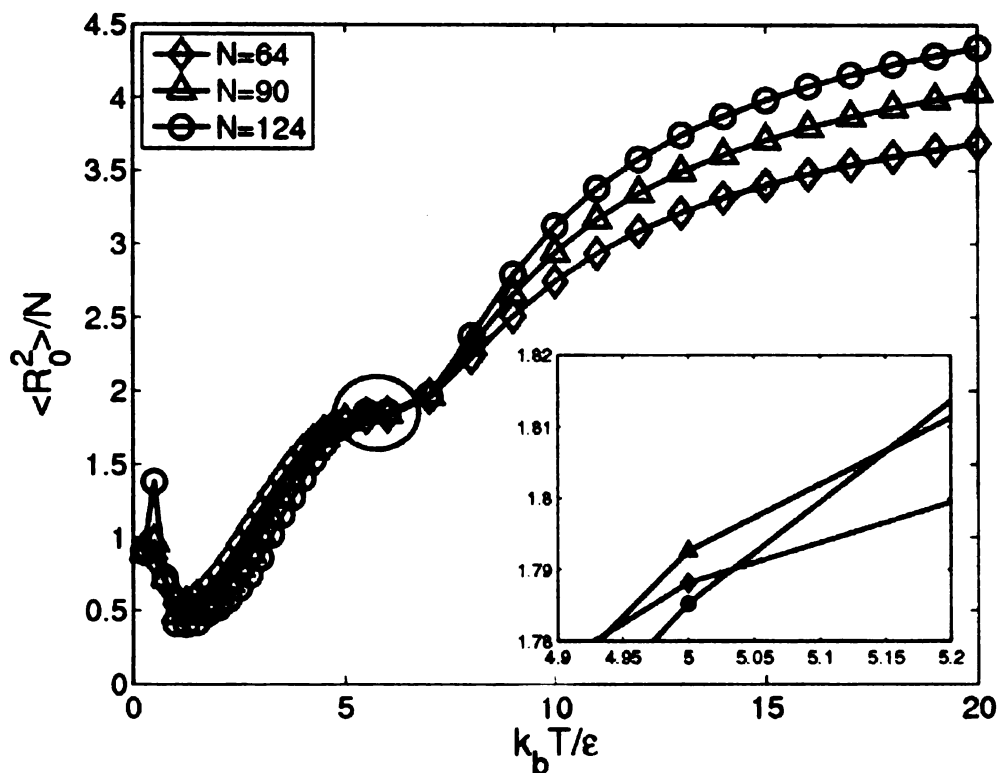


**Figure 3.10.**  $\langle R_0^2 \rangle / N$  versus temperature for different chain lengths ( $N= 64, 90, 124$ ). The crossing point for the length 90 and 124 chains gives a rough estimate of the  $\theta$  temperature for the model,  $T_\theta \approx 5.15$ .

To compare with experiment, we need a relation between the model and experimental temperatures. We assume that the experimental height increase begins at the  $\theta$  point in the model, and that this occurs at about  $T^\epsilon = 413\text{K}$ . We thus obtain  $\epsilon = k_B T^\epsilon / T^m = 80k_B$ , so the highest experimental temperature of  $473\text{K}$  corresponds in the simulation to  $T^m = 5.9$ . Examining the inset of Fig. 3.9b we see that the simulated macromolecules increase their height by about 0.8 monomer diameters between  $T_\theta = 5.15$  and  $T = 5.9$ . This agrees remarkably well with the experimental data, as a PS Kuhn segment is  $\approx 1$  nm in size.

### 3.5 Conclusion

Solvent and temperature strongly affect the conformations of polystyrene macromolecules and nanoparticles adsorption on a substrate. Measurements using AFM were used to study the conformations of polystyrene macromolecules and nanoparticles on selected substrates. We have observed interplay between the solvents used during deposition for the macromolecules and an irreversible height transition at low temperatures for both macromolecules and nanoparticles. We have also presented experimental evidence for a softening effect occurring near 40°C. As temperature increases the measured AFM height of the particles decreases. This softening effect can be attributed to the decrease in surface tension of polystyrene as temperature increases. This can be explained by looking at the scale of a single macromolecule and nanoparticle from that of the bulk. Using a simple model we found that ~50% of the monomer units are on the outer area of the particle. The energy to remove one of these monomer units is much less than from the bulk of the particle, suggesting that the temperature at which the particle can deform is less than that for bulk polystyrene. We can also use the JKR theory and the assumption that the particles adopt a spherical cap conformation to determine how the change in surface tension of the polystyrene affects the modulus of the particles. As temperature increases the modulus decreases for both macromolecules and nanoparticles.

In final experiments, several heat cycles to 75°C were performed on the extremely cross-linked polystyrene nanoparticles and it was determined that after each cycle the nanoparticle gradually reduces in height. This gradual decrease can be contributed to the adsorption of monomers onto the substrate with each heat cycle.

We have also presented experimental evidence for an expansion of single PS chains on a substrate as the temperature is increased. The height increase is due in part to the dynamics of the deposition process, in that the chains may not be fully equilibrated when initially deposited on the substrate. However, the height data are very consistent with an expansion in chain dimensions due to the globule to coil transition taking place in the adsorbed chain. Monte Carlo simulations were used to generate and analyze the configurations and heights of single chains on a surface, with parameters based on the experimental system. From the simulations we find that the change in height due to the globule to coil transition is of the same order as measured experimentally.

## Chapter 4: Directional Self Assembly: Nanoparticles Drawn to Carbon Nanotubes

### 4.1 Introduction

Assembling arrays of nanostructures is an integral component to this possible data storage technology. Forming arrays of nanoparticles has been approached using numerous methods including chemical modification of nanostructures,<sup>21</sup> self assembly,<sup>57, 58</sup> and nanolithography.<sup>59-61</sup> In one case electron beam lithography was used to create patterned hole and trench templates in a silicon substrate. A drop of gold nanoparticle suspension was then placed onto the patterned substrate and capillary forces served as the driving force to move the nanoparticles into the trenches.<sup>61</sup>

In this work we look at aligning nanoparticles with the aid of single-wall carbon nanotubes (SWNTs) which certainly has utility beyond our proposed application. *A posteriori* we find the nanotubes pull the nanoparticles to them during deposition and so by assembling or strategically locating the nanotubes one could then assemble nanoparticles in a unique and robust manner. Extensive research has already been performed on the alignment of nanotubes with modifications during SWNT synthesis used to promote alignment.<sup>62-64</sup> SWNTs are grown from a silica substrate coated with catalytic metal nanoparticles with subsequent chemical vapor deposition. Initially they will be perpendicular to the substrate, but as growth continues they will eventually lay down on the substrate forming an array of nanotubes that are parallel to the surface.

Currently, researchers can align nanoparticles on both single walled and multi-walled nanotubes through chemical modification of the nanotubes.<sup>65-68</sup> In one case CdSe nanoparticles were attached to acid-chloride modified SWNTs by amide bond formation.<sup>66</sup> Researchers have also attached nanoparticles to carbon nanotubes using

dielectrophoresis.<sup>69</sup> In this work SWNTs were linked between a Au/Ti electrode bilayer on a chip. A sinusoidal ac voltage was applied to the system after suspensions of polystyrene and gold nanoparticles were deposited onto the chips. The dielectrophoresis force applied to the system caused the nanoparticles to agglomerate to the nanotubes. Without the applied voltage the nanoparticles did not appear to attach to the nanotubes.

In this study, we are able to attach a variety of nanoparticles to SWNTs without the aid of specific chemical modification or dielectrophoresis. The nanoparticles are attracted to the nanotubes through van der Waals forces enhanced from the geometrical effects of the cylindrical nanotubes.

## 4.2 Experimental

Functionalized SWNTs were synthesized using the HiPco process.<sup>70, 71</sup> This process is a gas phase method that uses an iron catalyst to catalytically disproportionate high pressure CO gas to generate a mixture of metallic and semi-conductive SWNTs. The direction the graphene sheet is rolled determines whether the nanotube will be conductive or semi-conductive.<sup>72</sup> The SWNTs used in our experiments was functionalized with a butyl group via alkylation<sup>73</sup> and this functional group produces a poor conducting nanotube. The butyl group was added so that the SWNTs would be soluble in chloroform. Even so, in all experiments, the solution was sonicated for 30 minutes prior to sample preparation to ensure proper dissolution. The nanotube solutions were then spin coated at 5000 rpm for 40 seconds onto the selected substrates which included mica and silicon wafers.

Several nanoparticles were used for alignment along the SWNTs: polystyrene (PS), gold (Au), and cadmium selenide (CdSe). A detailed description of the nanoparticles characteristics can be found in Chapter 2, section 2.2 and in previous work.<sup>12, 74</sup> We also used polystyrene macromolecules which were standards purchased from Scientific Polymer Products, Inc. and had a weight average molecular weight of 393 kD and a polydispersity index of 1.2.

The Au nanoparticles were purchased from Meliorum Technologies and were suspended in toluene by having an unknown steric layer that is ~1.5 nm thick. We determined their average height via AFM to be  $7.5 \pm 1.0$  nm and so we believe the gold core was ~6.5 nm in diameter consistent with transmission electron microscopy (TEM) measurements. The CdSe nanoparticles<sup>75</sup> contain a steric layer of pyridine<sup>76</sup> that is

approximately 0.5 nm in length and are suspended in pyridine. Table 4.1 contains characteristic details for the nanoparticles used in these experiments. Note that the diameter listed for the polystyrene nanoparticles and molecules was predicted assuming the macromolecule collapses to a sphere with the bulk density of polystyrene ( $\rho \sim 1.04 \text{ g/cm}^3$ ) through  $D = [6M_n / \pi N_A \rho]^{1/3}$ , where  $N_A$  is Avogadro's number and  $M_n$  is the number average molecular weight. The diameter listed for the Au and CdSe nanoparticles was determined via AFM height.

**Table 4.1.** Sample Code, Number Average Molecular Weight (kD), Solvent, Diameter if the Macromolecules or Nanoparticles Collapse to the Bulk Density of Polystyrene and the AFM Height (Diameter) of Au and CdSe NPs.

Sample Code	Mn(kD)	PDI	Solvent	D (nm)
T-PS211k	211.0	1.3	benzene, toluene	8.6
T-PS78k	78.0	1.1	benzene	6.2
E-PS33k	33.0	1.9	benzene, chloroform	4.7
PS393k	339.0	1.2	benzene, toluene	10.1
Au	---	---	toluene	$7.5 \pm 1.0$
CdSe	---	---	pyridine	$4.5 \pm 0.5$

We prepared (0.1 – 10  $\mu\text{g/mL}$ ) solutions of all nanoparticles described above in the solvents given in Table 4.1. All solutions were sonicated for approximately 30 minutes and then deposited onto a substrate that contained SWNTs which were previously deposited by spin coating. The solutions were then imaged via AFM after the solvent had evaporated.

Surface profile measurements were performed with a Pacific Nanotechnology Nano-R atomic force microscope in close contact (oscillating) mode to generate height images that were not altered other than a simple leveling procedure. Silicon tips with a

spring constant of 25-75 N/m, tip curvature <10 nm, and a resonance frequency of 200-400 kHz were used for all experiments.

Transmission electron microscopy was also used to examine the alignment of nanoparticles on nanotubes. The samples were prepared by depositing a drop of SWNT solution onto a formvar supported TEM grid. Once the solvent had evaporated a drop of solution containing the nanoparticles was deposited on the grid. The polystyrene nanoparticles were then negatively stained with 1% phosphotungstic acid. The other nanoparticles were not stained since they provide sufficient electron contrast to be seen via TEM. The samples were then imaged with a JEOL 100CX TEM.

### 4.3 Results and Discussion

AFM and TEM images provide evidence of nanoparticle alignment on single-wall carbon nanotubes. The nanoparticles appear to agglomerate to the nanotubes on both freshly cleaved mica (surface energy,  $\gamma \approx 300$  mN/m) and silicon wafers ( $\gamma \approx 70$  mN/m), which indicate that surface energy does not play a role in the alignment for these rather high energy substrates. AFM and TEM images of the nanoparticles' alignment on nanotubes are revealed in Figs 4.1 and 4.2 respectively. Note that a few of the SWNTs agglomerate into small bundles (~10 nm). The SWNTs were deposited on a silicon wafer and are shown in Fig. 4.1a to reveal a rather randomly oriented array. Following the procedure outlined above, the E-33kD PS nanoparticles were deposited from chloroform on mica, the T-PS211k nanoparticles were deposited from benzene on a silicon wafer, and the Au nanoparticles were deposited from toluene on mica in Fig. 4.1b, c, and d. Note that for all substrates (silicon wafer and mica), all solvents (benzene, toluene, chloroform and pyridine), and all nanoparticle systems (Au NPs, PS NPs, and CdSe NPs) nanoparticle agglomeration onto the nanotubes was found as seen in the figure.

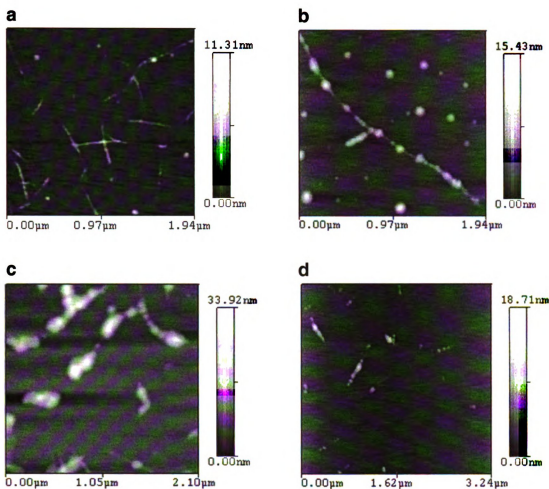


**Figure 4.1.** AFM height images of (a) SWNTs spin coated onto a silicon wafer, (b) E-PS33kD NPs deposited from chloroform on mica (c) T-PS211kD NPs deposited from benzene on a silicon wafer (d) Au NPs deposited from toluene on mica. Note that for the AFM images in b,c, and d the SWNTs were deposited onto the selected substrate prior to nanoparticle deposition.

TEM images of the nanoparticle alignment are shown in Figure 4.2. The images in Figure 4.2a and b are of Au NPs and SWNTs. The Au NPs appear to agglomerate to the nanotubes, but the large agglomerations of NPs do not as readily. As shown below the vdW interaction between the SWNT and nanoparticles decreases as the size of the nanoparticle increases. This suggests that the nanoparticles were agglomerated in the solvent prior to deposition on the surface. Shown in Figure 4.2c is a TEM image of a line

of CdSe nanoparticles on a nanotube and d is an image of the T-211kD PS NPs on the SWNTs. The polystyrene nanoparticles must be stained in order to be visualized by TEM, which causes a shadow effect that is not as visually appealing as micrographs for the other systems; however, we believe there is an agglomerate of the polystyrene nanoparticles present along the nanotubes.

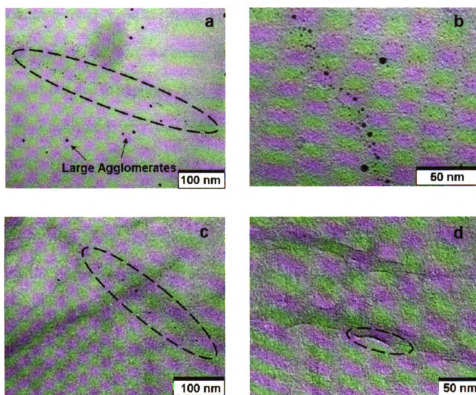


**Figure 4.2.** (a) and (b) TEM images of Au NPs aligned along SWNTs. (c) CdSe nanoparticles aligned along SWNTs and (d) T-211kD PS NPs agglomerated along SWNTs.

To explain this phenomenon we first considered the actions of the nanoparticles as they settle to the substrate. A droplet containing the nanoparticles in solvent is placed on the substrate already containing nanotubes. The benzene wets the substrates (both mica and silicon wafer) and as the particle moves to the substrate we suggest, as discussed below, they are attracted toward the SWNTs. Since the benzene wets the

substrate there is no pinning line to force the nanoparticles to deposit on the outer edge of the droplet to produce the behavior referred to as the coffee ring effect.<sup>77, 78</sup> During the coffee ring effect a ring of particles is created due to evaporation at the droplet's edge which causes a pinned contact line. Solvent from the center of the droplet replaces solvent lost by evaporation at the edge of the droplet; thus carrying particles to the droplet edge through capillary flow. In our work the solvents wet the substrates, which prevent a pinning line from occurring suggesting that the nanoparticles' alignment on the nanotubes is not due to capillary flow.

To understand why the nanoparticles are attracted to the carbon nanotubes, consider the system depicted in Fig. 4.3. The nanoparticle diffuses freely in the solvent above the substrate. As the solvent begins to evaporate, the particle is forced closer to the substrate as well as the nanotube, and is drawn to them by van der Waals forces. By analyzing the relative strengths of these forces one can show that the particle will tend to be pulled preferentially toward the nanotube as the solvent evaporates and is mediated by a combination of geometric and dielectric factors.

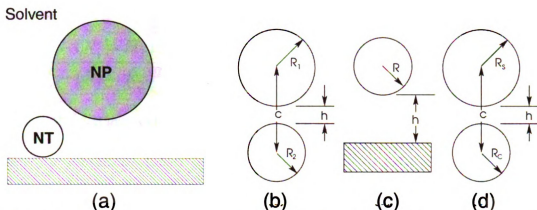


**Figure 4.3.** (a) Spherical nanoparticle (NP) diffusing in solvent near a nanotube (NT) on a substrate. (b-d) Coordinate systems for the geometries used in our systems: (b) sphere/sphere (c) sphere/plate and (d) sphere/cylinder.

The interaction potential and force between a sphere and cylinder and sphere and flat plane (substrate) can be determined using the Hamaker approach and pairwise summation of all involved intermolecular forces. The van der Waals interaction energy between two bodies  $U_{12}$  was first expressed by Hamaker<sup>79</sup> as

$$U_{12} = -C\rho_1\rho_2 \int_{V_1} dV_1 \int_{V_2} dV_2 \frac{1}{r^6} \quad (4.1)$$

where  $\rho_1$ ,  $\rho_2$ ,  $V_1$ , and  $V_2$  are the atom number densities and the total volumes of the objects,  $r$  is the distance between the volume elements, and  $C$  is the substance dependent London-van der Waals constant.

We are interested in three particular geometric combinations: two spheres, a sphere and plate and a sphere with a cylinder since these roughly describe the nanoparticle/nanoparticle, nanoparticle/substrate and nanoparticle/nanotube interactions. The potential energy between two spheres with radii  $R_1$  and  $R_2$  is given by<sup>79, 80</sup>

$$U_{SS}(c; R_1, R_2) = -\frac{A_{132}}{3} \left[ \frac{R_1 R_2}{c^2 - (R_1 + R_2)^2} + \frac{R_1 R_2}{c^2 - (R_1 - R_2)^2} + \frac{1}{2} \ln \frac{c^2 - (R_1 + R_2)^2}{c^2 - (R_1 - R_2)^2} \right] \quad (4.2)$$

where  $c$  is the distance between their centers (see Fig. 4.3b) and  $A_{132}$  is the Hamaker constant for substances 1 and 2 in the medium 3. In our calculations, we will use  $h=c-R_1-R_2$ , the distance to contact as our measure. From the sphere/sphere calculation it is possible to obtain the sphere/plate energy by taking one of the radii as infinity resulting in

$$U_{SP}(h; R) = -\frac{A_{132}}{6} \left[ \frac{R}{h} + \frac{R}{2R+h} + \ln \frac{h}{2R+h} \right] \quad (4.3)$$

where  $R$  is the sphere radius,  $h$  is the distance to contact and  $A_{132}$  is the effective Hamaker constant between the sphere 1 and plate 2 in the medium 3. The geometry for this case is shown in Fig. 4.3c.

For the nanoparticle/nanotube potential, we treat the cylinder as infinitely long since nanotube aspect ratios are typically  $\geq 1000$  and so the relation describing this system reduces to a single integral which must be evaluated numerically<sup>81, 82</sup>

$$U_{SC}(c, R_S, R_C) = -A_{132} \int_{-R_C}^{c+R_C} \arccos\left(\frac{r^2 + c^2 + R_C^2}{2rc}\right) \frac{R_S^3}{r^2 - R_S^2} r dr \quad (4.4)$$

where  $R_S$  and  $R_C$  are the sphere and cylinder radii, respectively,  $c$  is the distance between their centers,  $c = h + R_S + R_C$ , and  $A_{132}$  is the Hamaker constant. The coordinate system for this system is depicted in Fig. 4.3d.

To progress further the effective Hamaker constants for our system<sup>17, 80</sup> must be determined. For the polystyrene/nanotube/*SiO*<sub>2</sub> system in benzene, we need the parameter given in Table 4.2. These constants are for two bodies of the same composition acting across vacuum and to account for the effect of the solvent, we use the following approximation

$$A_{132} \approx (\sqrt{A_{11}} - \sqrt{A_{33}})(\sqrt{A_{22}} - \sqrt{A_{33}}) \quad (4.5)$$

where  $A_{ii}$  is the self Hamaker constant in vacuum.

**Table 4.2.** Hamaker constants for typical substances used in our experiments.

Substance	Hamaker Constant $A$ ( $zJ$ )
Benzene <sup>17</sup>	5.0
Polystyrene <sup>17</sup>	6.6
<i>SiO</i> <sub>2</sub> <sup>17</sup>	25
Nanotube <sup>83</sup>	50

For the polystyrene/nanotube/*SiO*<sub>2</sub> system in benzene we calculated the effective Hamaker constants as well as the potential energies at a distance of  $h = 0.5\text{\AA}$ . The results are tabulated in Table 4.3 along with the pertinent geometries where we assumed the spheres had a radius of 4 nm and the cylinder had a radius of 1 nm, which correspond approximately to the experimental measures of the nanoparticles and nanotubes.

**Table 4.3.** Hamaker constants and energies for typical substances and geometries used in our experiments.

<b>Substance</b>	<b>Geometry</b>	$A_{132}(zJ)$	$U_{12}(0.5\text{\AA}) (zJ)$
<i>SiO</i> <sub>2</sub> /Benzene/Polystyrene	Plate/Sphere	0.92	-0.86
Nanotube/Benzene/ Polystyrene	Cylinder/Sphere	1.6	-0.43
Polystyrene/Benzene/ Polystyrene	Sphere/Sphere	0.11	-0.040

By knowing the effective Hamaker constants, one may evaluate the potential energy as a function of the closest distance between the two bodies,  $h$  as shown in Fig. 4.4. In this figure the combined effect of geometry and interaction strength can be seen. The cylinder sphere potential is remarkably strong due in part to its geometry, but also because the dispersion force is stronger between carbon and polystyrene than *SiO*<sub>2</sub> and polystyrene.

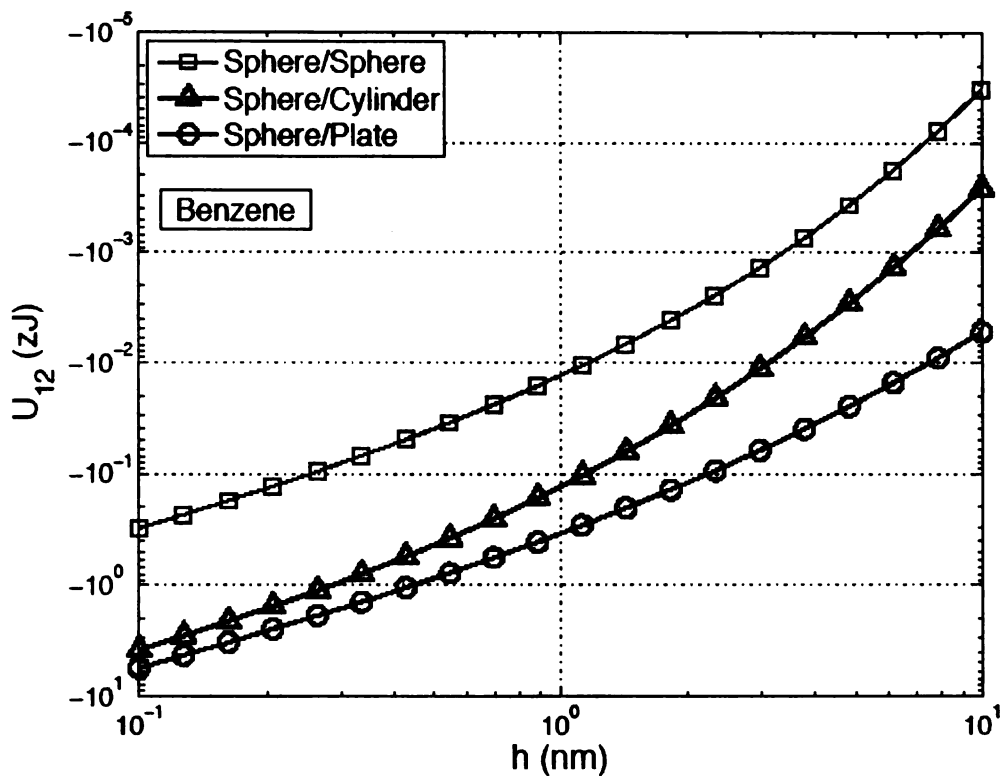


**Figure 4.4.** Van der Waals potential energies for two body systems. In all cases, the spheres are polystyrene, the cylinders are carbon nanotubes and the substrate (plate) is SiO<sub>2</sub>.

From our calculations it is easy to see why the nanoparticles are attracted to the nanotubes—there is a 150% gain in energy for doing so. Furthermore, the sphere/cylinder interaction potential is extremely high validating the rather large structures seen in Fig. 4.1. So, as the nanoparticles are drawn toward the nanotube others are more likely to follow. Similar effects have been studied using ultrafine fibers and aerosol particles.<sup>84</sup> As the solvent is evaporating the fibers act like a filtration system that captures the particles and pulls at them via their relatively strong van der Waals interaction.

#### **4.4 Conclusion**

As the nanoparticles settle closer to the substrate they are focused to the carbon nanotubes through strong van der Waals forces. Using pairwise summation and the Hamaker approach we were able to predict the strength of the van der Waals interaction between the sphere and the nanotube compared to that of the sphere and the substrate. From our results we concluded that the van der Waals strength between a sphere and cylinder greatly increases as the particle gets closer to the substrate. This increase in van der Waals interaction drives the nanoparticles to collect onto the nanotubes, which creates an alignment of nanoparticles onto carbon nanotubes. By aligning carbon nanotubes we will be able to achieve an array of nanoparticles that could benefit the advances in future data storage devices and other possible nanodevices.

## Chapter 5: Embedding Nanoparticles into a Cross-linked Network

### 5.1 Introduction

Robustly attaching the nanoparticle to the substrate is an integral component to millipede technology. Since the nanoparticle will be deformed by an AFM tip, the nanoparticles must be robustly attached to the surface to prevent tip forces from disordering the nanoparticle array during deformation. Embedding the nanoparticles within a polymer film thinner than the nanoparticle diameter is one way to achieve this. However, this technology has other applications since others, are currently exploring the optical properties produced by embedding silver nanoparticles into polymer films for metal/semiconducting polymer systems.<sup>10, 11</sup> Silver is dispersed into vapor-deposited nylon thin films (~100 nm) through heat treatment and are studied using optical and vibrational spectroscopy<sup>10</sup> as well as transmission electron microscopy (TEM) to find that nanoparticles placed on the surface will homogeneously distribute throughout the film after annealing. One of these studies<sup>10</sup> was followed by another to find that chemical composition of the nanoparticles is critical in controlling dispersion.<sup>85</sup>

Teichroeb and Forrest have investigated embedding Au nanoparticles in a polymer film (~180 nm thick) by annealing the film above its glass transition temperature.<sup>86</sup> The Au nanoparticles were deposited on top of the film and as the system was heated the nanoparticles slowly fell into the film. Atomic force microscopy (AFM) was used to measure the height of the nanoparticles at different annealing times and as the annealing time increased the height of the Au nanoparticles decreased suggesting they slowly embedded into the polymer film. The interesting observation in this work was that the

nanoparticles were embedded into the film ~3-4 nm even when the film was at a temperature below the bulk glass transition.

In contrast to the above studies we investigate embedding polystyrene nanoparticles in a thin cross-linkable polymer film where the nanoparticle diameter is greater than the thickness of the polymer film, which allows creation of a memory device discussed above as well as a nano-rough surface. Researchers have recently begun to explore the effect of nano-rough surfaces (features <100nm) on surface wettability.<sup>87-91</sup> In one case swift ion irradiation was used to produce a random array of nanometer features on a surface.<sup>87</sup> It was discovered that as the defect concentration or roughness increased the hydrophobicity of the surface also increased. Meli and Lennox<sup>88</sup> have also seen an increase in hydrophobicity with increased roughness, but with highly regular gold nanoparticles and surface topology with roughness on the order of 10 nm in height. In this work we study the wetting behavior of a nanorough surface having features that are ~3 nm high with a unique system where the nanoparticles are chemically identical to the polymer film so roughness effects can be solely addressed.

## 5.2. Experimental

Polystyrene nanoparticles were used as a well characterized component and were synthesized according to the procedure of Harth, et al.<sup>15</sup> and kindly provided by Prof. Craig Hawker. A linear, random, copolymer precursor consisting of styrene monomer and benzocyclobutene (BCB) was first synthesized where the latter component dictates the degree of cross-linking. In this work we use a BCB level of 20 mol%, denoted as tightly (T) cross-linked. A dilute solution of the linear precursor polymer was then dripped into a hot solvent activating the intermolecular cross-linking reaction to create nanoparticles containing a single macromolecule whose size is dictated by the initial precursor molecular weight as well as the degree of cross-linking. The nanoparticles were prepared at concentrations of 50  $\mu\text{g/mL}$ , 100  $\mu\text{g/mL}$ , and 200  $\mu\text{g/mL}$  in benzene, since concentrations greater than 100  $\mu\text{g/mL}$  revealed agglomeration of the nanoparticles in the spin coated films discussed below. A PS25kD linear precursor containing 2.5 mol% BCB was used for the polymer film since it is chemically identical to the nanoparticles. Details of the nanoparticle system and linear precursor can be found in Table 5.1. Note, to ascertain the nanoparticle conformation on the substrate, we determined the diameter ( $D$ ) assuming the macromolecule collapses to a sphere with the bulk density of polystyrene ( $\rho \sim 1.04 \text{ g/cm}^3$ ) through

$$D = \left[ \frac{6M_n}{\pi N_A \rho} \right]^{1/3} \quad (5.1)$$

where  $N_A$  is Avogadro's number and  $M_n$  is the number average molecular weight.

**Table 5.1.** Sample, Molecular Mass, Polydispersity Index (PDI), Degree of Cross-linking, Nature (i.e. cross-linked or linear), and Diameter if the Linear Precursors or Nanoparticles Collapse to the Bulk Density of Polystyrene (Eq.5.1) for the Samples.

Sample Code	Mn (kD)	PDI	mol% cross-linking agent	diameter (nm)
PS25k	24.5	1.14	2.5	4.2
T-PS211k	211	1.32	20	8.6

Solutions of the linear precursor were prepared in benzene at a concentration of 5 mg/mL. The nanoparticles' solution at each concentration and linear precursor solution were mixed together in equal parts and then spin coated onto a Sigmacote™ silanized wafer at 5000 rpm for 40 seconds. Sigmacote™ (Sigma-Aldrich) is a solution consisting of 2.5% chlorosiloxane ((SiCl<sub>2</sub>C<sub>4</sub>H<sub>9</sub>)<sub>2</sub>O) and 97.5% heptane that functionalizes the surface with short alkane chains. During the spin coating process the wafer was flooded with the polystyrene solution and left to stand for ~2 minutes prior to starting the spin coater. This delay was required due to the low surface energy of the substrate and the requirements that a homogenous film must be manufactured. Note we used the silanized wafer as a convenient way to create an ultrathin polymer film (~5nm) since the same concentration spin coated onto a higher free energy substrate, such as a silicon wafer, would have produced a 40 nm thick film. In addition, the subsequent cross-linking procedure on a bare silicon wafer produced a highly adsorbed film that was difficult to characterize by the technique discussed below to determine its thickness. Furthermore, a higher energy substrate substantially deformed the nanoparticle used here.<sup>12</sup>

The samples were heated in an oven to 250°C for 30 minutes to produce a cross-linked network of polymer film that will firmly embed the nanoparticle within the film.

At 250°C the pendent cross-linking group (benzocyclobutene, BCB) along the linear precursor chain will bond with another cross-linking group to create a highly cross-linked network.

Surface profile measurements were performed with a Pacific Nanotechnology Nano-R atomic force microscope in close contact (oscillating) mode to generate height images that were not altered other than a simple leveling procedure. Silicon tips with a spring constant of 25-75 N/m, tip curvature of <10 nm, and a resonance frequency of 200-400 kHz were used for all experiments.

### 5.3. Results and Discussion

Initially only the linear precursor was spin coated onto the substrate and then imaged before and after heating to ensure a smooth film was present (Fig. 5.1a). A razor blade was used to create a thin scratch in the film which was subsequently imaged via AFM to determine the film thickness. The measured thickness was 5 nm and a line analysis of this is shown in Figure 5.1b. Below a thickness of 4 nm a continuous film was unattainable, which made it clear that only the T-PS211kD nanoparticle system (highest molecular weight nanoparticle system available to us)<sup>12</sup> would still be elevated enough to image after embedding.

The height of a bare T-PS211kD nanoparticle on a silanized wafer is ~8-9 nm (see Fig.5.2), suggesting an embedded particle will appear 3-4 nm in height. Note the systems were imaged before and after heat and they were heated to 250°C to activate the cross-linking process. The average height of the nanoparticles after the film was cured was  $\sim 2.6 \pm 0.4$  nm, which suggests that the particles were embedded within the film and that the nanoparticles were essentially in a spherical conformation within the film.

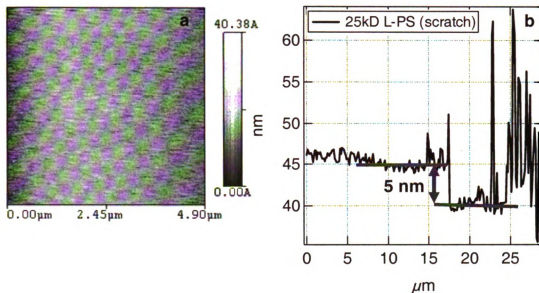


**Figure 5.1.** (a) AFM height image of PS25kD film on Sigmacote™ after being heated to 250°C for 30 min. (b) Line analysis of the scratch made in the film. The film appears to be 4-5 nm thick.

An AFM height image of the embedded T-PS211k nanoparticles in the cross-linked polystyrene film is shown in Figure 5.2 and 5.3. Nanoparticle concentrations of 50  $\mu\text{g}/\text{mL}$ , 100  $\mu\text{g}/\text{mL}$ , and 200  $\mu\text{g}/\text{mL}$  were used to see if roughness of the surface would increase with a greater number of nanoparticles embedded within the film. The number of nanoparticles per  $\mu\text{m}^2$  ( $n_p$ ) was calculated for the concentrations and was determined to be  $\sim 9$  for the 50  $\mu\text{g}/\text{mL}$  sample,  $\sim 16$  for the 100  $\mu\text{g}/\text{mL}$  sample, and  $\sim 3$  for the 200  $\mu\text{g}/\text{mL}$  sample. An AFM image of the nanoparticles prior to and after curing the film at the 50  $\mu\text{g}/\text{mL}$  concentration is shown in Fig. 5.3a and b. There was little to no change in the height after being heated. A height profile for the nanoparticles before and after embedment is shown in Fig. 5.2. The difference in height is  $\sim 5$ -6 nm, which suggests a film thickness of  $\sim 5$  nm. The sample was also dipped in benzene for  $\sim 1$  minute to

determine if the film or nanoparticles would dissolve away. Since the film is cross-linked the nanoparticles embedded within the film should remain intact and from the image in Fig. 5.2c it is clear that the nanoparticles and film did not dissolve.

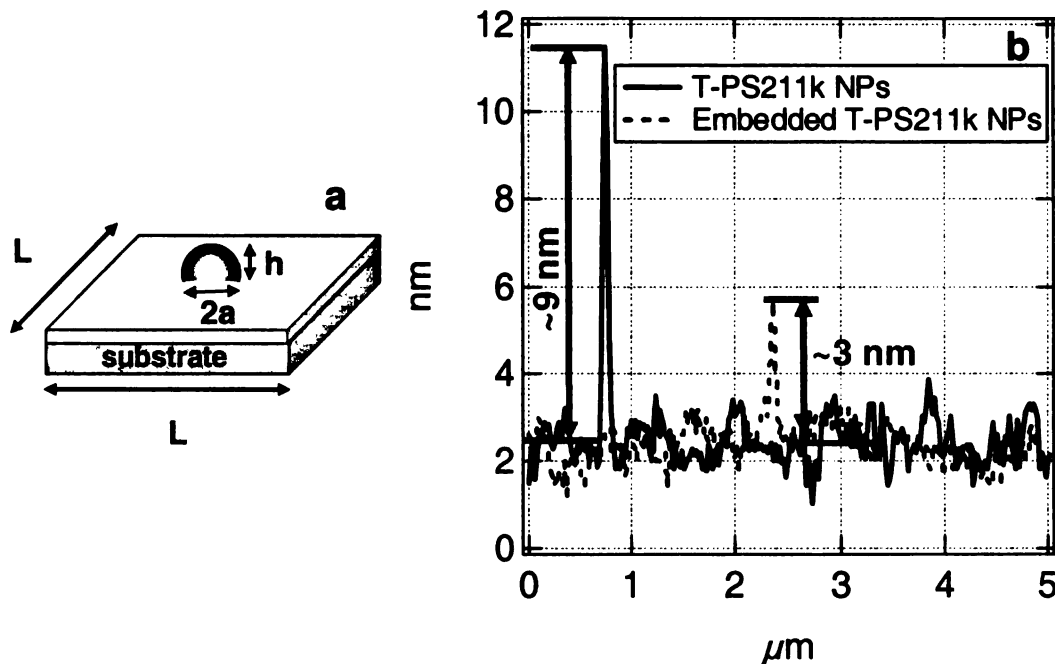


**Figure 5.2.** (a) Diagram of nanoparticle embedded in thin polymer film. (b) Graph of the height of a T-PS211k nanoparticle on Sigmacote™ before embedment (black line) and the height of a nanoparticle after embedment (dashed line). The average difference in height between these particles is  $\sim 5-6$  nm consistent with the film thickness determined in Fig. 5.1.

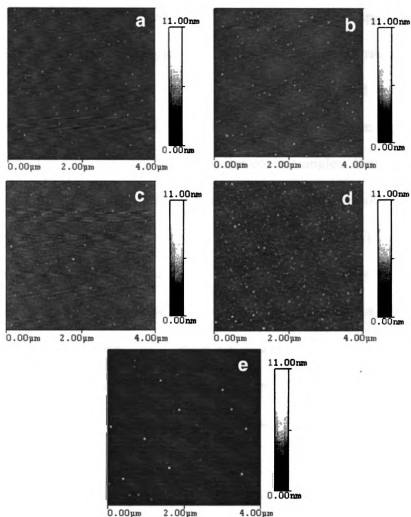


**Figure 5.3.** AFM height images of T-PS211k NPs embedded in a thin polymer film (PS25kD linear precursor). (a) Height image prior to cure ( $50 \mu\text{g/mL}$ ). (b) Height image after heating to  $250^\circ\text{C}$  for 30 minutes ( $50 \mu\text{g/mL}$ ). (c) Height image after the sample in b was dipped in benzene for 1 minute ( $50 \mu\text{g/mL}$ ). (d) Height image after heating to  $250^\circ\text{C}$  for 30 minutes ( $100 \mu\text{g/mL}$ ). (e) Height image after heating to  $250^\circ\text{C}$  for 30 minutes ( $200 \mu\text{g/mL}$ ).

The surface energy of the annealed polystyrene film and the higher concentration ( $100 \mu\text{g/mL}$ ) of embedded nanoparticles within the film were studied using contact angle measurements. The advancing ( $\theta_A$ ) and receding ( $\theta_R$ ) contact angles for both systems

were  $\theta_A = 89.0^\circ \pm 4.3$ ,  $\theta_R = 87.4 \pm 2.7$  and  $\theta_A = 81.1^\circ \pm 0.9$ ,  $\theta_R = 75.9 \pm 5.9$  for the cross-linked polystyrene film and the embedded nanoparticle film, respectively. Note the advancing and receding contact angles for the 50  $\mu\text{g/mL}$  concentration of embedded nanoparticles were essentially equal to the contact angles measured on the polystyrene film with no nanoparticles embedded,  $\theta_A = 89.7 \pm 3.0$  and  $\theta_R = 84.1 \pm 3.7$ . We note that a sample not discussed here, 10  $\mu\text{g/mL}$ , had similar contact angles, also, the samples spin coated and cured with 150 and 200  $\mu\text{g/mL}$  nanoparticle solutions showed contact angles of  $\sim 89^\circ$ , however, they showed phase separated regions (see Fig. 5.3e).

The wetting properties of rough surfaces<sup>92</sup> have been vastly explored by many researchers. They have found that as the roughness of the surface increases the surface energy of the surface increases,<sup>52, 93-95</sup> however, this increase in hydrophobicity occurs when the contact angle on the smooth surface is greater than  $90^\circ$ . Others have found that if the surface is initially hydrophilic (contact angle  $< 90^\circ$ ) then by increasing surface roughness, the contact angle will actually decrease creating a more hydrophilic surface.<sup>96, 97</sup> Bhushan and Jung<sup>97</sup> have considered the hydrophobic and hydrophilic nature of leaf surfaces to study the effect of microbumps (3-7 $\mu\text{m}$  in height) and nanobumps (70-780 nm in height) on the surface to find nanobumps had a greater effect on hydrophobicity than microbumps. Hydrophilic leaves were also studied to better understand roughness changes on hydrophilic surfaces where it was determined that as the roughness of hydrophilic surfaces increases the hydrophilicity increases.

Young's equation is used to determine the contact angle ( $\theta_s$ ) between a smooth solid surface and a liquid droplet and is expressed as<sup>92</sup>

$$\cos \theta_s = \frac{\gamma_s - \gamma_{SL}}{\gamma_L} \quad (5.3)$$

where  $\gamma_S$ ,  $\gamma_L$ ,  $\gamma_{SL}$  are the surface tensions of the solid-gas, liquid-gas, solid-liquid interfaces. Yet, Young's equation does not account for surface roughness effects and therefore would not apply to the polystyrene nano-rough surfaces described here. A model to describe roughness effects on hydrophobicity was first presented by Wenzel in 1936<sup>98</sup> to relate contact angles for a chemically homogenous yet rough surface using a roughness factor  $r_f$ ,

$$\cos \theta_r = r_f \cos \theta_s \quad (5.4)$$

where  $\theta_r$  is the contact angle on the rough surface.

The Wenzel model can be used to predict that when  $r_f$  increases the contact angle will decrease if  $\theta_s$  is less than  $90^\circ$ , which is what we found in our study although the amplitude of our roughness is  $\sim 3\text{nm}$ . The polystyrene film (with no nanoparticles) is a slightly hydrophilic surface with a contact angle less than  $90^\circ$ . When nanoparticles are embedded in the polymer film to increase roughness we see a decrease in contact angle by  $\sim 10^\circ$ . Using the advancing angles we can calculate Wenzel's prediction of  $r_f$  using eq. 5.4. For the high concentration of nanoparticles ( $100\mu\text{g/mL}$ ) we find an  $r_f$  value of 9.

The calculated  $r_f$  value can also be considered by using a spherical cap model to find the surface area of the nanoparticle embedded in the film. We first determine the contact diameter ( $2a$ ) of the nanoparticle embedded in the film (see Fig. 5.2a) using the surface area of a spherical cap ( $A_{SC}$ )

$$A_{SC} = \pi D h = \pi(a^2 + h^2) \quad (5.5)$$

where  $h$  is the height of the embedded nanoparticle ( $h \sim 3\text{nm}$ ), and  $D$  is the predicted nanoparticle diameter (eq. 5.1). The  $r_f$  value is the ratio of the actual area to the projected area and can be calculated from

$$r_f = \frac{A_{sc} + L^2 - \pi a^2}{L^2} \text{ where } L^2 = \frac{1}{n_p} \quad (5.6)$$

The calculated  $r_f$  value for the 100  $\mu\text{g/mL}$  sample is 1.0004, which is much less than the  $r_f$  value calculated from the Wenzel model (~9). This large variance in  $r_f$  suggests that nanoscale roughness has a large effect on wettability with the possibility of forming extremely hydrophilic surfaces. Note the Cassie and Baxter model extends the Wenzel model to heterogeneous surfaces.<sup>99, 100</sup> This model was also developed for both porous substrates and rough hydrophobic substrates and therefore does not apply to our particular case.

The contact angle hysteresis also plays a role in nano-rough surfaces. According to the Wenzel model as the roughness of the sample increases, the contact angle hysteresis should also increase. Contact angle hysteresis is the difference between the advancing and receding contact angle ( $\Delta\theta$ ). For the cross-linked polystyrene film this value is ~1.6 and for the embedded nanoparticles this value increased to ~5.2, suggesting that this increase in hysteresis due to increased roughness holds true for our system.<sup>88</sup>

#### **5.4. Conclusion**

In this work we were able to robustly attach the nanoparticles to the substrate by embedding them (locking them) into a cross-linkable film. The nanoparticles are now capable of being deformed by an AFM tip without being displaced.

Nanoparticles embedded in a polymer film created nano-rough surfaces that influenced the wettability of the polystyrene surface. Due to polystyrene's hydrophilic nature (contact angle  $<90^\circ$ ) the addition of polystyrene nanoparticles to create a nano-rough surface increased the hydrophilicity of the surface.

## **Chapter 6: Conclusions**

The conformation of intramolecularly cross-linked polystyrene nanoparticles on a solid substrate was investigated. Optimal rigidity of the nanoparticles on the substrate must be accomplished in order to achieve advancements in data storage systems. The substrates tested include a high energy mica surface and a low energy silanized silicon wafer. The nanoparticles collapse on the mica substrate, but remain robust and structured on the silanized wafer, yet, an extreme amount of cross-linking is required for the nanoparticles to retain their original spherical shape regardless of the substrate surface energy. The nanoparticle behavior was also observed at elevated temperatures to reveal that the height of the extremely cross-linked nanoparticles slowly decreases. The temperature where a rapid size change occurs was well below the bulk glass transition temperature.

Polystyrene macromolecules were also investigated at elevated temperatures and it was discovered that these macromolecules fluctuate between two conformational states: a collapsed state at low temperatures (25°C) and an expanded state at high temperatures (200°C). We used a combination of experiment and Monte Carlo molecular simulation to examine and explain this phenomenon.

Arrays of nanoparticles could then be produced by focusing them to SWNTs. As the nanoparticles settle closer to the substrate they are focused to the carbon nanotubes through strong van der Waals forces. The SWNT serves as a nucleation site that directs the nanoparticles to it.

The nanoparticles were then robustly attached to the substrate by embedding them within a cross-linked thin polystyrene film. Locking the nanoparticles in place allows one

to deform a single nanoparticle without displacing or disrupting the nanoparticle. Deformation of single nanoparticles is not currently achievable due to the limits of the AFM.

The items addressed in this work build a path for the possibility of nanoparticles being addressed as single bits of information along a surface for the advancement of molecular memory.

## Appendix A: Atomic Force Microscopy

Atomic force microscopy (AFM) was invented in 1986 by Binnig, et al.<sup>101</sup> The AFM reflects a laser from a solid state diode off a cantilever to a detector. A sharp probe located on the end of the cantilever moves over the surface of the sample while measurements of the signal changes in the bending of the cantilever are taken. A diagram of the AFM set-up is shown in Figure A.1

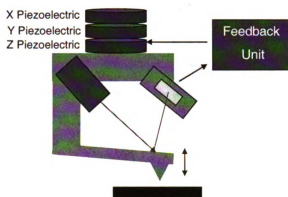


**Figure A.1.** Atomic force microscopy diagram that illustrates the laser being emitted from the diode to the cantilever and reflected back to the detector. The feedback unit uses the input signal to produce the voltage that drives the piezoelectric ceramic.

A Pacific Nanotechnology Nano-R atomic force microscope in close contact mode was used for all images presented in this work. Close contact (oscillating) mode produces four outputs: Z(error), Z(height), Z(sensor), and Z(demodulated). A list is provided below that contains a detailed description of each output.

**Z(error):** The cantilever deflection, as a function of the actuator position. This signal is used to determine if the tip has made contact with the sample.

**Z(height):** As the tip moves over the sample, it periodically taps the surface, while measurements of the signal changes in the bending of the cantilever are taken.

**Z(sensor):** This linearizes the Z(height) signal using the Z piezo. The Z(sensor) provides a more accurate height measurement than the Z(height) because it is linearized.

**Z(demodulated):** (phase image) Measures changes in phase angle during scanning due to energy dissipation during tip-sample interaction, which can be caused by changes in topography, tip-sample molecular interactions, deformation of the tip-sample contact, and experimental conditions. The phase image can also be used to determine if your tip is broken or has something stuck to it such as a dust particle or nanoparticle. The phase image can also determine if your sample is contaminated. Examples of good and bad phase images are shown in Figure A.3.

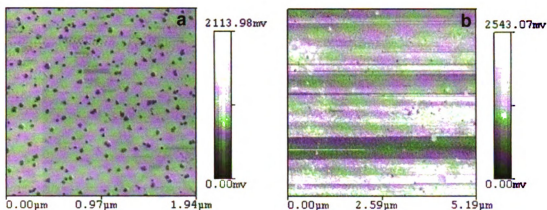


**Figure A.2.** (a) Example of a good AFM phase image of 33kD E-PS NPs. (b) Example of a bad phase image of 33kD E-PS NPs. Some of the particles in the image appear triangular which indicates the tip is broken. The streaks that appear in the phase image indicate that either the surface is contaminated (e.g. finger print) or something is stuck to the tip such as a dust particle or nanoparticle.

For all AFM experimental data presented in this work, the particle heights were determined by taking the average of 50 particles' heights; however, the lateral size could not be found due to convolution effects created by the tip.<sup>18, 19</sup>

AFM tip damage before and after scanning was also investigated. Scanning electron microscopy (SEM) was used to determine if the tip was damaged after tip approach and after scanning a freshly cleaved mica substrate. SEM images of the AFM tip at 3 different stages is shown in Figure A.3a, b, and c. An example of a damaged AFM tip is shown in Figure A.3d. The damaged tip is rounded on the end suggesting that the tip was damaged during tip approach or sample contact.

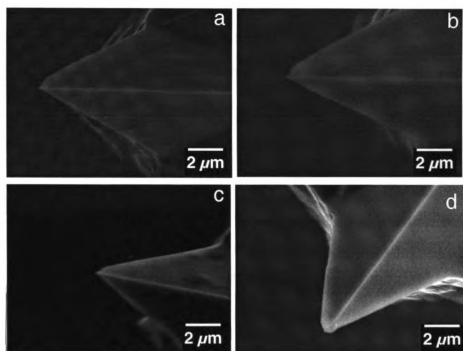


**Figure A.3.** (a) AFM tip prior to tip approach. (b) AFM tip after tip approach. (c) AFM tip after scanning a mica substrate. (d) Damaged AFM tip.

AFM calibration for lateral resolution was performed using a calibration grid. Since the particles imaged for this work were less than 10 nm, gold nanoparticles (Au NPs) were used to calibrate the AFM in the vertical direction. Au NPs were purchased from Meliorum Technologies and are suspended in toluene. The particles average height via AFM was  $\sim 7$  nm. We use these particles to ensure that the measured height values for other particles are accurate.

A hot stage was designed for the Nano-R AFM so that individual molecules and nanoparticles could be observed at elevated temperatures. The hot stage consisted of a solid metal cylindrical sample puck with an alumina insulator, heater element, and thermocouple connected to a PID controller to monitor the temperature (see Figure A.4). AFM scans at temperatures above room temperature require that the hot stage be turned

off during scanning due to electrical interference effects; therefore, the high temperature experiments have a temperature range of approximately  $\pm 5^{\circ}\text{C}$  as the heater cools slightly during AFM scans. In all AFM elevated temperature experiments the sample and AFM components were kept at the desired temperature for  $\sim 3$  hours to ensure that all components, specifically tip and sample, had reached the desired temperature, which aided in the prevention of thermal drift.

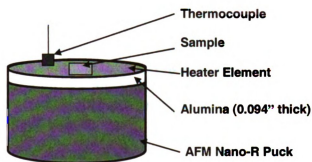


**Figure A.4.** AFM heater design. Samples can be heated to a maximum temperature of  $100^{\circ}\text{C}$  without damaging the AFM.

Calibration of the hot stage was performed by imaging Au NPs spin coated on a mica substrate at temperatures ranging from  $25^{\circ}\text{C}$  to  $75^{\circ}\text{C}$ . At each temperature the average AFM height of the Au NPs was  $\sim 7$  nm.

The final task of this research is to indent a single nanoparticle via an AFM tip. Unfortunately due to limitations of the AFM this was not achievable. In an attempt to indent a nanoparticle on a single-walled nanotube it was discovered that the AFM x-y resolution was not accurate. AFM images of nanoparticles and SWNTs before and after tip indentation is shown in Figure A.5. The circled area designates where the tip should have struck the sample and the dotted circle is the debris from where the tip actually struck the sample.

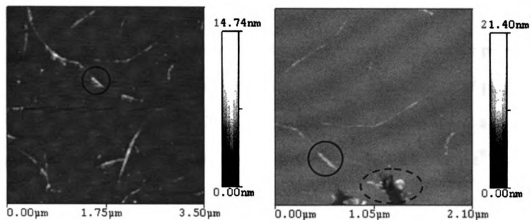


**Figure A.5.** (a) AFM height image of nanoparticles aligned on single-walled nanotubes before tip approaches sample (b) AFM height image of nanoparticles aligned on single-walled nanotubes after tip approaches sample. In both (a) and (b) the black circle represents the targeted tip approach area and in (b) the dotted circle represents where the tip actually struck the sample.

## **Appendix B: Height vs. Temperature Data for Polystyrene Macromolecules and Nanoparticles**

The graphs displayed below contain height vs. temperature data for polystyrene macromolecules and nanoparticles. Figures B.1 and B.2 contain graphs of polystyrene macromolecules that were heated from 25°C to 75°C. In both cases a softening temperature occurs at ~ 40°C. Both samples were sprayed onto a Sigmacote™ substrate from a solvent/non-solvent solution.

Nanoparticle height vs. temperature data can be found in Figures B.3 and B.4. Both of these systems were drop deposited onto a Sigmacote™ substrate in benzene. In both cases a softening effect at ~ 40°C is observed.

A graph of the 393kD macromolecules is shown in Figure B.5. The macromolecules were heated in an oven to 200°C to 75°C for 30 cycles. The values plotted in the graph are for heights after cycles 20 and 30. This proves that the macromolecule fluctuation is still observed after several cycles. Heat cycles between 200°C and 75°C were also performed on the polystyrene nanoparticles. The AFM height of the 211kD T-PS NPs was observed for 3 heat cycles and is plotted in Figure B.6. The nanoparticles were deposited in pure solvent (benzene) and in solvent/non-solvent (benzene/2-MEA).

Fourier transform infrared spectroscopy (FTIR) and X-ray photoelectron spectroscopy (XPS) were performed to prove that 2-MEA was not present in the sample after initial preparation. Figures B.7 and B.8 contain FTIR and XPS spectrums of the sample after initial preparation of the 393kD polystyrene macromolecules in benzene/2-MEA. Both spectrums reveal that there is no residual solvent or non-solvent still present after initial preparation.

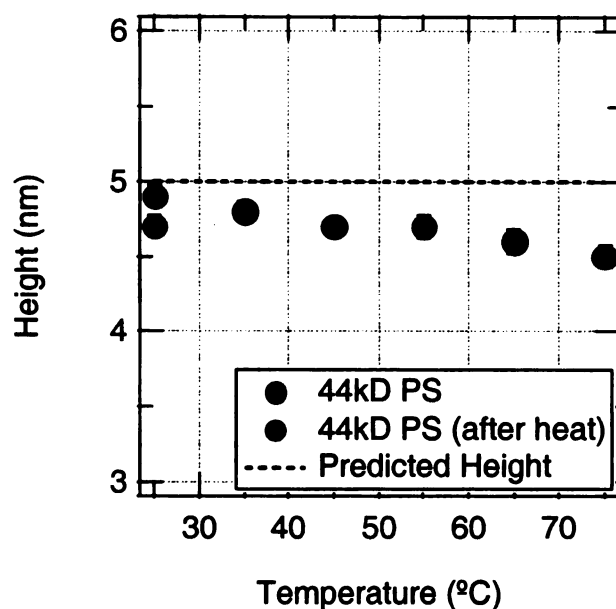


**Figure B.1.** Height vs. temperature for 44kD polystyrene macromolecules heated from 25°C to 75°C. The sample was spray deposited from a solvent/non-solvent solution onto a silanized wafer.

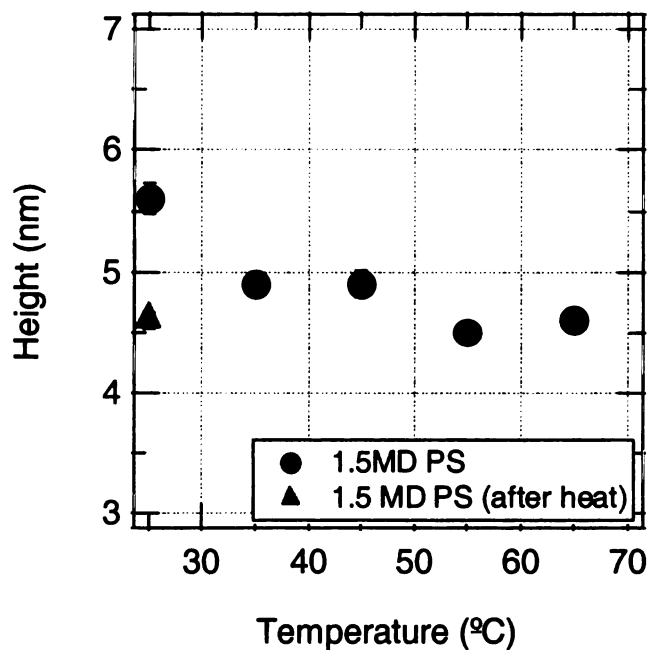


**Figure B.2.** Height vs. temperature for 1.5MD polystyrene macromolecules heated from 25°C to 75°C. The sample was spray deposited from a solvent/non-solvent solution onto a silanized wafer.

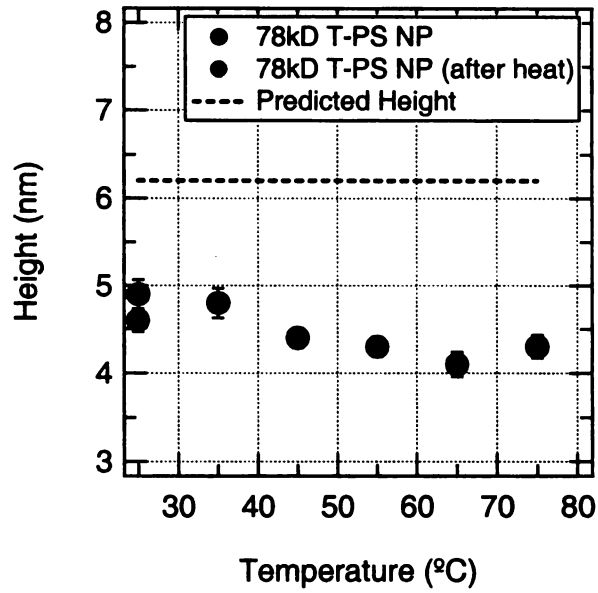


**Figure B.3.** Height vs. temperature for 78kD T-PS nanoparticles heated from 25°C to 75°C. The sample was drop deposited onto a silanized wafer from benzene.

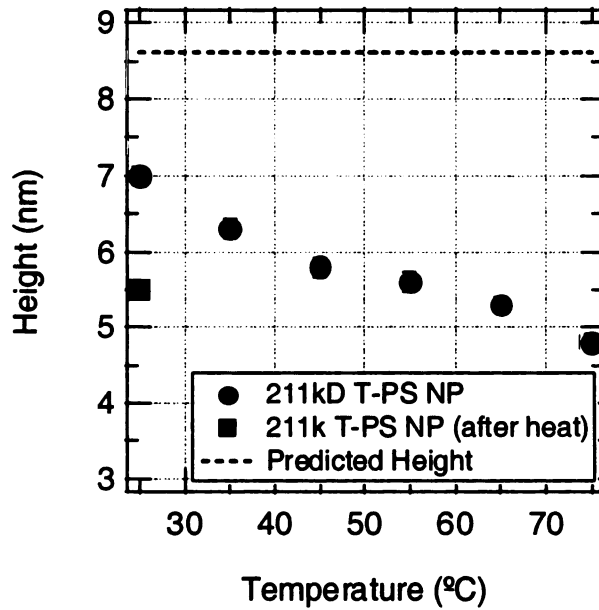


**Figure B.4.** Height vs. temperature for 211kD T-PS nanoparticles heated from 25°C to 75°C. The sample was drop deposited onto a silanized wafer from benzene.

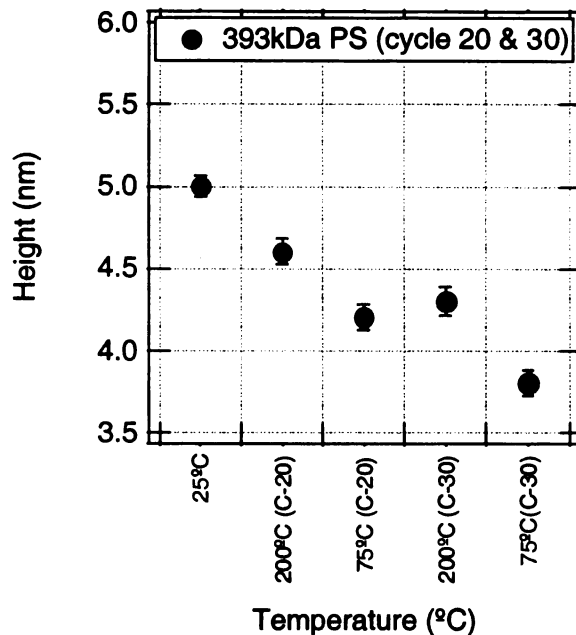


**Figure B.5.** Height of 393kD PS macromolecules at room temperature after being heated to the corresponding temperatures on the graph. The height of the macromolecules fluctuates as the temperature is cycled between 75°C and 200°C. The graph shows the heights obtained after cycles 20 and 30.

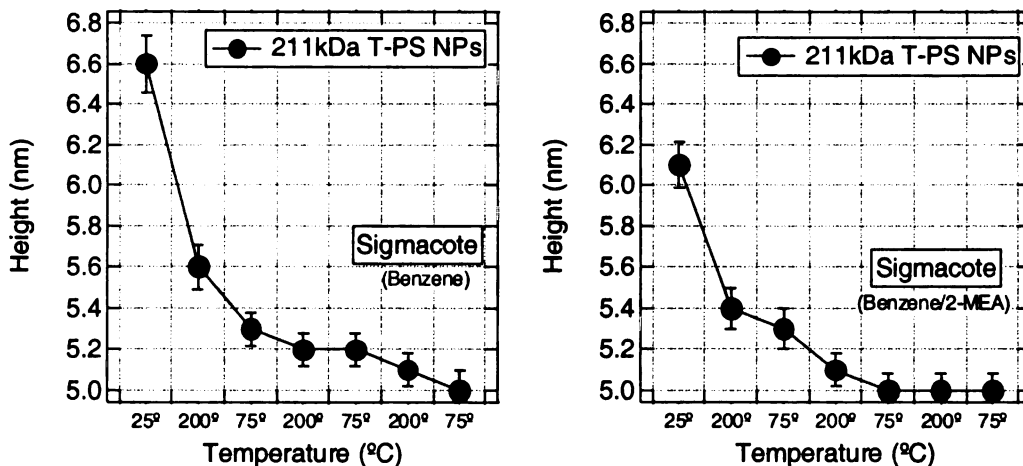


**Figure B.6.** Height vs temperature graphs of the 211kD T-PS NP system. (a) NPs were deposited in pure benzene and (b) NPs were deposited in benzene/2-MEA. The nanoparticles do not undergo the same two phase behavior that is observed in the macromolecules.

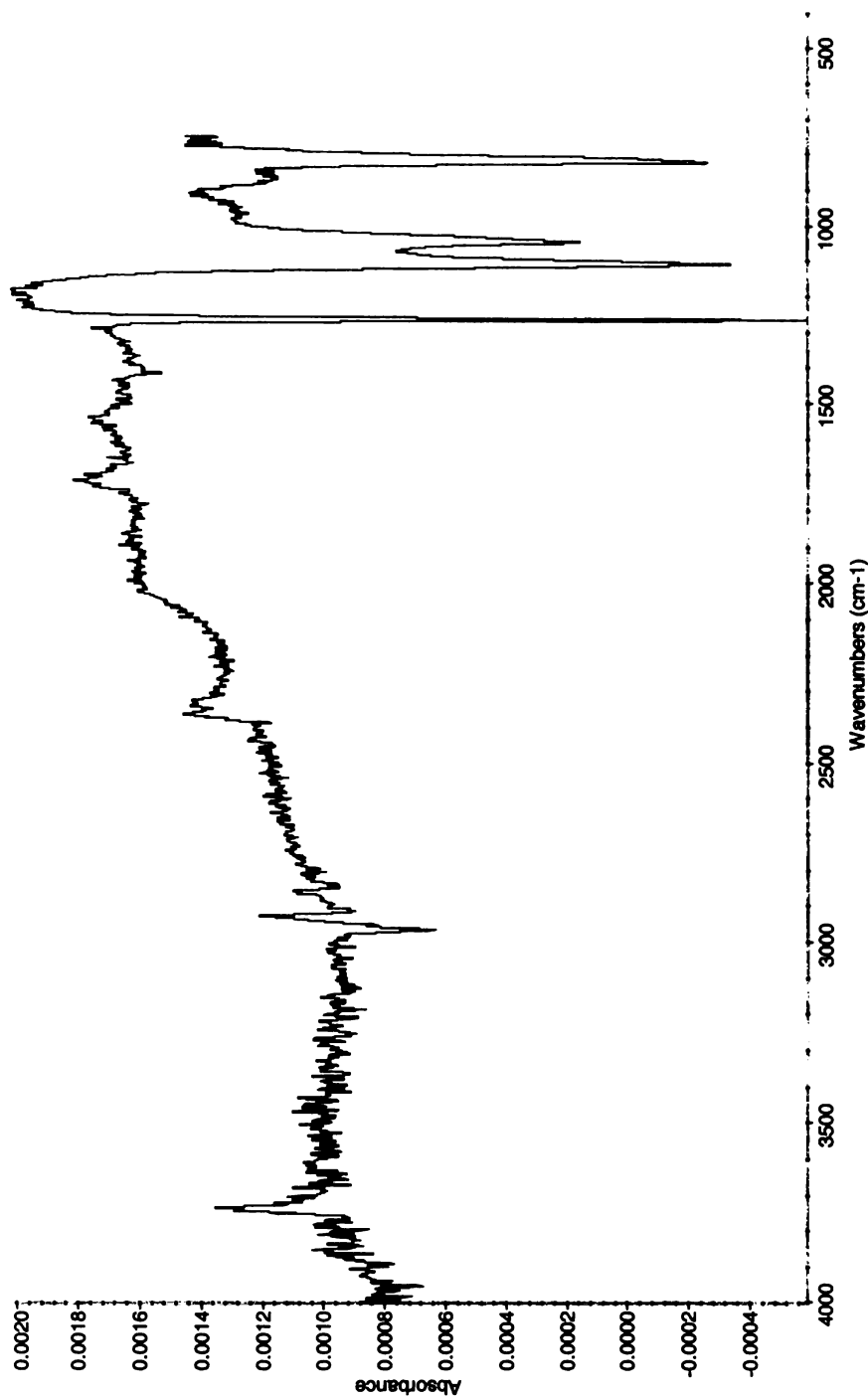


**Figure B.7.** FTIR spectrum of 393kD PS macromolecules directly after preparation. A 0.1  $\mu\text{g}/\text{mL}$  solution of 70% benzene/30% 2-MEA was sprayed onto a silanized wafer. Only polystyrene peaks are present in the scan, there is no trace of residual solvent or non-solvent.

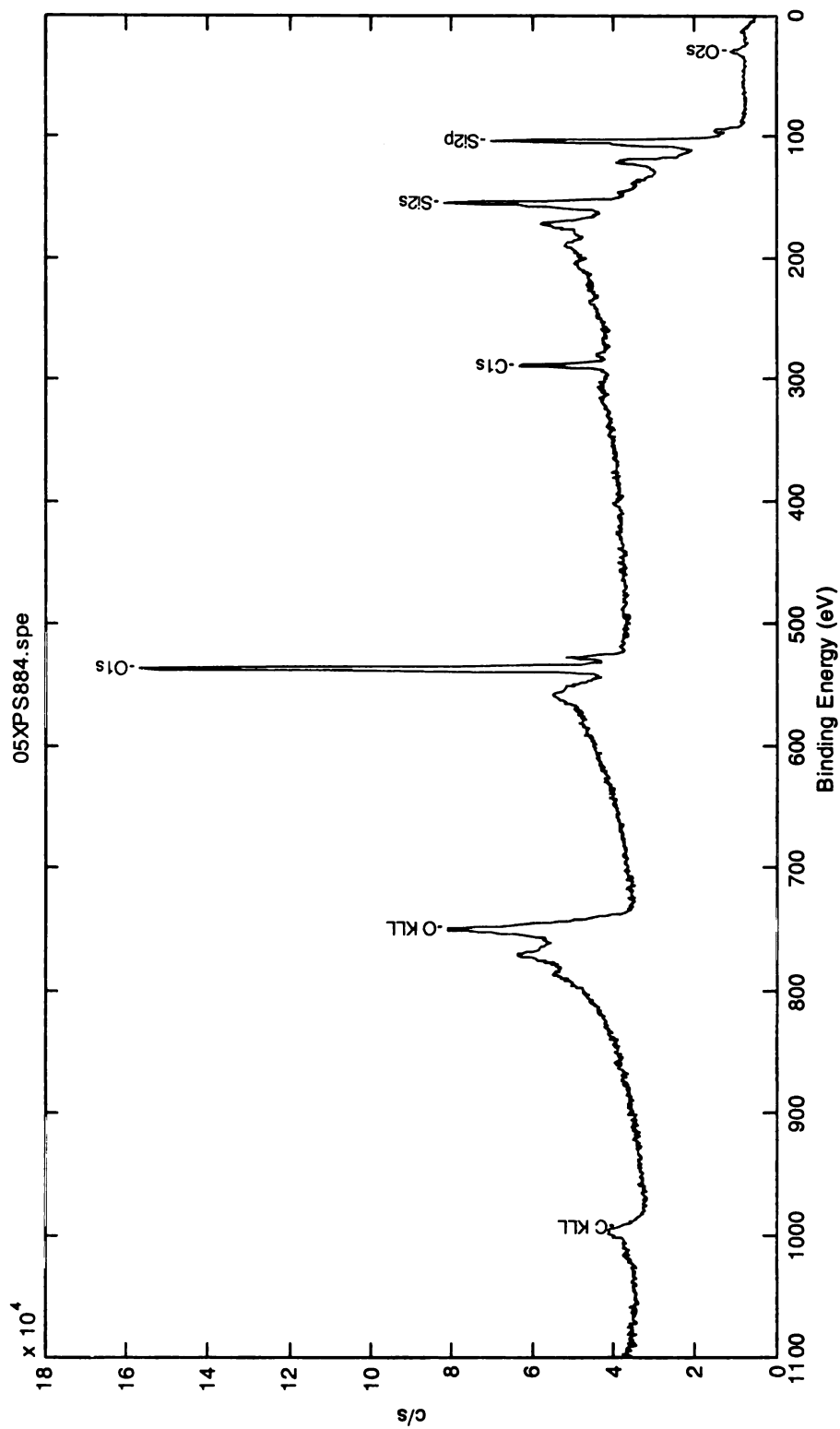


**Figure B.8.** XPS spectrum of 393kD PS macromolecules directly after preparation. A 0.1  $\mu\text{g/mL}$  solution of 70% benzene/30% 2-MEA was sprayed onto a silanized wafer. The silanized wafer was used for the background. There is no trace of any residual solvent or non-solvent.

## References

1. Vettiger, P.; Cross, G.; Despont, M.; Drechsler, U.; Durig, U.; Gotsmann, B.; Haberle, W.; Lantz, M. A.; Rothuizen, H. E.; Stutz, R.; Binnig, G. K. *Nanotechnology, IEEE Transactions on* **2002**, 1, (1), 39-55.
2. Eleftheriou, E.; Antonakopoulos, T.; Binnig, G. K.; Cherubini, G.; Despont, M.; Dholakia, A.; Durig, U.; Lantz, M. A.; Pozidis, H.; Rothuizen, H. E.; Vettiger, P. *IEEE Transactions on Magnetics* **2003**, 39, (2), 938-945.
3. Durig, U.; Cross, G.; Despont, M.; Drechsler, U.; Haberle, W.; Lutwyche, M. I.; Rothuizen, H.; Stutz, R.; Widmer, R.; Vettiger, P.; Binnig, G. K.; King, W. P.; Goodson, K. E. *Tribology Letters* **2000**, 9, (1-2), 25-32.
4. Vettiger, P.; Despont, M.; Drechsler, U.; Durig, U.; Haberle, W.; Lutwyche, M. I.; Rothuizen, H. E.; Stutz, R.; Widmer, R.; Binnig, G. K. *Ibm Journal of Research and Development* **2000**, 44, (3), 323-340.
5. Mackay, M. E. *IEEE Transactions on Nanotechnology* **2005**, 4, (5), 641-644.
6. Xue, G.; Lu, Y.; Shi, G.; Dai, Q. *Polymer* **1994**, 35, (4), 892-894.
7. Rana, N.; Yau, S.-T. *Nanotechnology* **2004**, 15, (3), 275-278.
8. Teranishi, T.; Sugawara, A.; Shimizu, T.; Miyake, M. *J. Am. Chem. Soc.* **2002**, 124, (16), 4210-4211.
9. Mathur, A.; Brown, A. D.; Erlebacher, J. *Langmuir* **2006**, 22, (2), 582-589.
10. Akamatsu, K.; Tsuboi, N.; Hatakenaka, Y.; Deki, S. *J. Phys. Chem. B* **2000**, 104, (44), 10168-10173.
11. Porel, S.; Singh, S.; Harsha, S. S.; Rao, D. N.; Radhakrishnan, T. P. *Chem. Mater.* **2005**, 17, (1), 9-12.
12. Durette, T. E.; Mackay, M. E.; VanHorn, B.; Wooley, K. L.; Drockenmuller, E.; Malkoch, M.; Hawker, C. J. *Nano Lett.* **2005**, 5, (9), 1704-1709.
13. Zhang, Q.; Clark, C. G.; Wang, M.; Remsen, E. E.; Wooley, K. L. *Nano Lett.* **2002**, 2, (10), 1051-1054.
14. Richardson, M. J. *Journal of Polymer Science: Part C* **1965**, (3), 21-29.
15. Harth, E.; Horn, B. V.; Lee, V. Y.; Germack, D. S.; Gonzales, C. P.; Miller, R. D.; Hawker, C. J. *J. Am. Chem. Soc.* **2002**, 124, (29), 8653-8660.
16. Israelachvili, J. N.; Alcantar, N. A.; Maeda, N.; Mates, T. E.; Ruths, M. *Langmuir* **2004**, 20, (9), 3616-3622.

17. Israelachvili, J. N., *Intermolecular and Surface Forces*. Academic Press: 1992.
18. Ebenstein, Y.; Nahum, E.; Banin, U. *Nano Lett.* **2002**, 2, (9), 945-950.
19. Markiewicz, P.; Goh, M. C. *Langmuir* **1994**, 10, (1), 5-7.
20. Mecke, A.; Lee, I.; Baker, J. R.; Holl, M. M. B.; Orr, B. G. *The European Physical Journal E* **2004**, 14, 7-16.
21. Chubynsky, M. V.; Thorpe, M. F. *Current Opinion in Solid State and Materials Science* **2001**, 5, (6), 525-532.
22. Johnson, K. L.; Kendall, K.; Roberts, A. D. *Proceedings of the Royal Society of London. Series A, Mathematical and Physical Sciences* **1971**, 324, (1558), 301-313.
23. Kendall, K.; Padget, J. C. *International Journal of Adhesion and Adhesives* **1982**, 2, (3), 149-154.
24. Fowkes, F. M. *Ind. Eng. Chem.* **1964**, 56, (12), 40-52.
25. Dee, G. T.; Sauer, B. B. *Colloidal Interface Science* **1992**, 152, (1), 85-103.
26. Ferry, J. D., *Viscoelastic Properties of Polymers*. 3rd ed.; John Wiley & Sons: 1980; p 672.
27. Rubenstein, M.; Colby, R. H., *Polymer Physics*. Oxford University Press: 2003; p 440.
28. Dobrynin, A. V.; Deshkovski, A.; Rubinstein, M. *Physical Review Letters* **2000**, 84, (14), 3101.
29. Dobrynin, A. V.; Rubinstein, M. *Macromolecules* **2002**, 35, (7), 2754-2768.
30. G. Xue, Y. L., G. Shi, and Q. Dai. *Polymer* **1994**, 35, (4), 892-894.
31. Mundra, M. K.; Ellison, C. J.; Behling, R. E.; Torkelson, J. M. *Polymer* **2006**, 47, (22), 7747-7759.
32. Priestley, R. D.; Ellison, C. J.; Broadbelt, L. J.; Torkelson, J. M. *Science* **2005**, 309, (5733), 456-459.
33. See, Y. K.; Cha, J.; Chang, T.; Ree, M. *Langmuir* **2000**, 16, (5), 2351-2355.
34. Shin, H. S.; Jung, Y. M.; Oh, T. Y.; Chang, T.; Kim, S. B.; Lee, D. H.; Noda, I. *Langmuir* **2002**, 18, (15), 5953-5958.
35. Serghei, A.; Tress, M.; Kremer, F. *Macromolecules* **2006**, 39, (26), 9385-9387.

36. Erichsen, J.; Dolgner, K.; Zaporojtchenko, V.; Faupel, F. *Macromolecules* **2004**, *37*, (24), 8813-8815.
37. Fryer, D. S.; Peters, R. D.; Kim, E. J.; Tomaszewski, J. E.; de Pablo, J. J.; Nealey, P. F.; White, C. C.; Wu, W. I. *Macromolecules* **2001**, *34*, (16), 5627-5634.
38. Giessibl, F. J.; Quate, C. F. *Physics Today* **2006**, *59*, (12), 44-50.
39. Sugden, S. *Journal of the Chemical Society* **1924**, *125*, 32-41.
40. de Gennes, P., *Scaling Concepts in Polymer Physics*. Cornell University: Ithaca, 1979.
41. Netz, R. R.; Andelman, D. *ArXiv: cond-mat/0002266* **2000**, *1*, pp. 1-44.
42. Frenkel, D. a. B. S., *Understanding Molecular Simulation*. 2002; Vol. Academic Press.
43. Hammersley, J. M.; Handscomb, D. C., *Monte Carlo Methods*. John Wiley & Sons, Inc.: New York, 1964.
44. A. Michel, S. K., and B. Wunderlich In *Molecular dynamics simulations of the adsorption of single chains on surfaces.*, 12th annual workshop, Recent developments in computer simulation studies in condensed matter physics, 2000; 2000.
45. Flory, P. J., *Statistical Mechanics of Chain Molecules*. Interscience Publishers: 1969.
46. Chandrasekhar, S. *Reviews of Modern Physics* **1943**, *15*, (1), 1.
47. Doye, J. P. K.; Sear, R. P.; Frenkel, D. *Journal of Chemical Physics* **1998**, *108*, (5), 2134-2142.
48. Bachmann, M.; Janke, W. *Physical Review Letters* **2005**, *95*, (5), 058102-4.
49. Rajesh, R.; Dhar, D.; Giri, D.; Kumar, S.; Singh, Y. *Physical Review E* **2002**, *65*, (5), 056124.
50. K. Binder, J. B. M. M. W. P. F. R. *Macromolecular Symposia* **2006**, *237*, (1), 128-138.
51. Grassberger, P. *Physical Review E* **1997**, *56*, (3), 3682.
52. Liu, Y.; Chen, X.; Xin, J. H. *Nanotechnology* **2006**, *17*, (13), 3259-3263.
53. Rosenbluth, M. N.; Rosenbluth, A. W. *The Journal of Chemical Physics* **1955**, *23*, (2), 356-359.

54. Wall, F. T.; Erpenbeck, J. J. *The Journal of Chemical Physics* **1959**, 30, (3), 634-637.
55. Wall, F. T.; Erpenbeck, J. J. *The Journal of Chemical Physics* **1959**, 30, (3), 637-640.
56. Binder, K.; Baschnagel, J.; Müller, M.; Paul, W.; Rampf, F. *Macromolecular Symposia* **2006**, 237, (1), 128-138.
57. Sohn, B. H.; Choi, J. M.; Yoo, S. I.; Yun, S. H.; Zin, W. C.; Jung, J. C.; Kanehara, M.; Hirata, T.; Teranishi, T. *J. Am. Chem. Soc.* **2003**, 125, (21), 6368-6369.
58. Jang, J.; Oh, J. H. *Langmuir* **2004**, 20, (20), 8419-8422.
59. Haynes, C. L.; McFarland, A. D.; Smith, M. T.; Hulteen, J. C.; Van Duyne, R. P. *J. Phys. Chem. B* **2002**, 106, (8), 1898-1902.
60. Cui, Y.; Bjork, M. T.; Liddle, J. A.; Sonnichsen, C.; Boussert, B.; Alivisatos, A. P. *Nano Lett.* **2004**, 4, (6), 1093-1098.
61. Kuo, C. W.; Shiu, J. Y.; Chen, P. *Chem. Mater.* **2003**, 15, (15), 2917-2920.
62. Huang, S.; Woodson, M.; Smalley, R.; Liu, J. *Nano Lett.* **2004**, 4, (6), 1025-1028.
63. Kusunoki, M.; Rokkaku, M.; Suzuki, T. *Applied Physics Letters* **1997**, 71, (18), 2620-2622.
64. Li, W. Z.; Xie, S. S.; Qian, L. X.; Chang, B. H.; Zou, B. S.; Zhou, W. Y.; Zhao, R. A.; Wang, G. *Science* **1996**, 274, (5293), 1701-1703.
65. Banerjee, S.; Wong, S. S. *J. Am. Chem. Soc.* **2003**, 125, (34), 10342-10350.
66. Haremza, J. M.; Hahn, M. A.; Krauss, T. D.; Chen, S.; Calcines, J. *Nano Lett.* **2002**, 2, (11), 1253-1258.
67. Ou, Y. Y.; Huang, M. H. *J. Phys. Chem. B* **2006**, 110, (5), 2031-2036.
68. Zanella, R.; Basiuk, E. V.; Santiago, P.; Basiuk, V. A.; Mireles, E.; Puente-Lee, I.; Saniger, J. M. *J. Phys. Chem. B* **2005**, 109, (34), 16290-16295.
69. Zheng, L.; Li, S.; Brody, J. P.; Burke, P. J. *Langmuir* **2004**, 20, (20), 8612-8619.
70. Chiang, I. W.; Brinson, B. E.; Huang, A. Y.; Willis, P. A.; Bronikowski, M. J.; Margrave, J. L.; Smalley, R. E.; Hauge, R. H. *J. Phys. Chem. B* **2001**, 105, (35), 8297-8301.
71. Nikolaev, P.; Bronikowski, M. J.; Bradley, R. K.; Rohmund, F.; Colbert, D. T.; Smith, K. A.; Smalley, R. E. *Chemical Physics Letters* **1999**, 313, (1-2), 91-97.

72. McEuen, P. L.; Fuhrer, M. S.; Hongkun, P. *Nanotechnology, IEEE Transactions on* **2002**, 1, (1), 78-85.
73. Saini, R. K.; Chiang, I. W.; Peng, H.; Smalley, R. E.; Billups, W. E.; Hauge, R. H.; Margrave, J. L. *J. Am. Chem. Soc.* **2003**, 125, (12), 3617-3621.
74. Tuteja, A.; Mackay, M. E.; Hawker, C. J.; Van Horn, B.; Ho, D. L. *Journal of Polymer Science Part B: Polymer Physics* **2006**, 44, (14), 1930-1947.
75. Asokan, S.; Krueger, K. M.; Alkhalid, A.; Carreon, A. R.; Mu, Z. Z.; Colvin, V. L.; Mantzaris, N. V.; Wong, M. S. *Nanotechnology* **2005**, 16, (10), 2000-2011.
76. Skaff, H.; Emrick, T. *Chemical Communications* **2003**, (1), 52-53.
77. Deegan, R. D.; Bakajin, O.; Dupont, T. F.; Huber, G.; Nagel, S. R.; Witten, T. A. *Nature* **1997**, 389, (6653), 827-829.
78. Deegan, R. D.; Bakajin, O.; Dupont, T. F.; Huber, G.; Nagel, S. R.; Witten, T. A. *Physical Review E* **2000**, 62, (1), 756.
79. Hamaker, H. C. *Physica* **1937**, 4, (10), 1058-1072.
80. Parsegian, V. A., *van der Waals Forces*. Cambridge University Press: New York, 2006.
81. Kirsch, V. A. *Advances in Colloid and Interface Science* **2003**, 104, (1-3), 311-324.
82. Rosenfeld, J. I.; Wasan, D. T. *Journal of Colloid and Interface Science* **1974**, 47, (1), 27-31.
83. Snow, E. S.; Campbell, P. M.; Novak, J. P. *Applied Physics Letters* **2002**, 80, (11), 2002-2004.
84. Kirsh, V. A. *Colloid Journal* **2004**, 66, (4), 444-450.
85. Akamatsu, K.; Kawamura, T.; Nabika, H.; Deki, S.; Strunskus, T.; Faupel, F. *Journal of Materials Chemistry* **2002**, 12, (12), 3610-3614.
86. Teichroeb, J. H.; Forrest, J. A. *Physical Review Letters* **2003**, 91, (1), 016104.
87. Ramos-Canut, S. *Nuclear Instruments and Methods in Physics Research Section B: Beam Interactions with Materials and Atoms* **2006**, 245, (1), 322-326.
88. Meli, M. V.; Lennox, R. B. *Langmuir* **2007**, 23, (4), 1619-1622.
89. G. R. J. Artus, S. J. J. Z. H. P. G. K. M. S. S. *Advanced Materials* **2006**, 18, (20), 2758-2762.

90. Cao, B.-Y.; Chen, M.; Guo, Z.-Y. *Physical Review E (Statistical, Nonlinear, and Soft Matter Physics)* **2006**, 74, (6), 066311-7.
91. Rios, P. F.; Dodiuk, H.; Kenig, S.; McCarthy, S.; Dotan, A. *Journal of Adhesion Science and Technology* **2006**, 20, (6), 563-587.
92. Adamson, A. W.; Gast, A. P., *Physical Chemistry of Surfaces*. 6 ed.; John Wiley & Sons, Inc: New York, 1997; p 358.
93. McHale, G.; Shirtcliffe, N. J.; Newton, M. I. *Langmuir* **2004**, 20, (23), 10146-10149.
94. Lundgren, M.; Allan, N. L.; Cosgrove, T.; George, N. *Langmuir* **2003**, 19, (17), 7127-7129.
95. Shastry, A.; Case, M. J.; Bohringer, K. F. *Langmuir* **2006**, 22, (14), 6161-6167.
96. Cheng, Y.-T.; Rodak, D. E.; Angelopoulos, A.; Gacek, T. *Applied Physics Letters* **2005**, 87, (19), 194112-3.
97. Bhushan, B.; Jung, Y. C. *Nanotechnology* **2006**, 17, (11), 2758-2772.
98. Wenzel, R. N. *Ind. Eng. Chem.* **1936**, 28, (8), 988-994.
99. Baxter, S.; Gregg, S. J.; Razouk, R. I.; Hirst, W.; Adam, N. K.; Crisp, D. J.; Cassie, A. B. D.; Shuttleworth, R.; Kembal, C.; Barkas, W. W.; Nieuwenhuis, K. J.; Schofield, R. K.; Foster, A. G.; Gregg, S. J.; Bond, R. L.; Ashpole, D. K.; Maggs, F. A. P.; Wark, I. W.; Bangham, D. H.; Joly, M.; Hirst, W.; Griffith, M.; Dresel, E. M.; Duncan, J. F.; Neale, S. M.; Barrer, R. M.; Razouk, R. I.; Atkinson, D. I. W.; Klinkenberg, A.; Pearse, J. F.; Brinkman, H. C.; Ernst, E.; Hartley, G. S.; Denbigh, K. G.; Childs, E. C. *Discussions of the Faraday Society* **1948**, 3, 94-&.
100. Cassie, A. B. D.; Baxter, S. *Transactions of the Faraday Society* **1944**, 40, 0546-0550.
101. Binnig, G.; Quate, C. F.; Gerber, C. *Physical Review Letters* **1986**, 56, (9), 930.

MICHIGAN STATE UNIVERSITY LIB



3 1293 02956 1